The Pennsylvania State University

The Graduate School

Graduate Program in Petroleum and Natural Gas Engineering

SIMULATION OF SECONDARY MIGRATION IN FAULTS:

DYNAMIC CONTROLS ON HYDROCARBON COLUMN HEIGHT

A Thesis in

Petroleum and Natural Gas Engineering

by

Matthew Hamilton Bennett

Submitted in Partial Fulfillment
of the Requirements
for the Degree of

Master of Science

December 1996

I grant The Pennsylvania State University the nonexclusive right to use this work for the University's own purposes and to make single copies of the work available to the public on a not-for-profit basis if copies are not otherwise available.

Matthew Hamilton Bennett

We approve the thesis of Matthew Hamilton Bennett.

Date of Signature
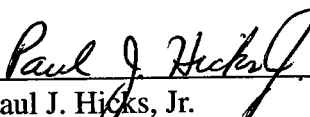
Paul J. Hicks

Paul J. Hicks, Jr.
Assistant Professor of Petroleum and Natural
        Gas Engineering
Thesis Co-Adviser

Sept. 6, 1996
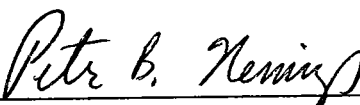
Peter B. Flemings

Peter B. Flemings
Assistant Professor of Geosciences
Thesis Co-Adviser

Sept 6, 1996

Turgay Ertekin

Turgay Ertekin
Professor of Petroleum and Natural
        Gas Engineering
Section Chair of Petroleum and Natural
        Gas Engineering

Sept 6 '96

Abstract

Secondary migration through fault zones and the concurrent charging of reservoirs in juxtaposition with these zones is modeled using analytical and numerical techniques. The steady-state hydrocarbon column heights that result from this process are controlled by the petrophysical properties of the fault zone, the flux of oil into the fault zone, and the geometry of the reservoir. In the analytical model, steady-state column height is a function of fault zone properties and oil flux into the fault zone. Similarly, in the numerical model steady-state column height is a function of fault zone properties, oil flux into the fault zone, and reservoir geometry. Six models are developed investigating variations in hydrocarbon column height. The first model illustrates the application of static methodologies where hydrocarbon column height is a function of capillary pressure. The second and third models show hydrocarbon column height as a dynamic function only of oil flux into the fault zone when the ratio of column height to reservoir thickness is small. Hydrocarbon column height as a function of reservoir geometry is illustrated in the fourth and fifth models where finite reservoirs are incapable of being charged to full potential when the ratio of analytical column height to reservoir thickness is high. The sixth model is analogous to more complex geological systems, where a broad range of column heights are predicted and the effects of petrophysical differences within that fault zone are investigated.

Table of Contents

List of Figures

List of Tables

Nomenclature

Roman

A = cross sectional area of the fault zone

g = gravitational acceleration

G = geometrical pore factor

h = height above the free water level

h_{oil} = height of the hydrocarbon column

$J(S_w)$ = Leverett-J function

k = intrinsic pemeability

k_{ro} = relative permeability to oil

k_{rw} = relative permeability to water

L = length of the fault zone

P_c = capillary pressure

P_d = capillary entry pressure

P_{FWL} = pressure at the free water level

P_o = oil pressure

P_w = water pressure

Q_o = volumetric oil flow rate

S_o = oil saturation

S_w^a = adjusted water saturation

| S_w | = | water saturation |
| S_{wirr} | = | irreducible water saturation |

Greek

Φ_o	=	oil potential
μ_o	=	oil viscosity
ρ	=	density
θ	=	angle from vertical of the fault zone
σ	=	interfacial tension between oil and water
ϕ	=	porosity
ρ_o	=	oil density
ρ_w	=	water density

ACKNOWLEDGMENTS

I would like to express my sincerest thanks to Dr. Paul J. Hicks and Dr. Peter B. Flemings, for their patience, guidance, enthusiasm and encouragement throughout the course of this work. I am deeply indebted to the both of them for serving as my advisors on this project. A graduate student could not ask for two finer role models.

In addition, I would like to thank Dr. Turgay Ertekin for his review of this manuscript. His comments provided a fresh and knowledgeable perspective that improved the quality of this thesis.

I would also like to thank the Petroleum and Natural Gas Engineering section at Penn State and the Exxon Production Research Company for their financial support of my graduate studies and this thesis. I am particularly indebted to the contributions of Chris Shaw and Bill Symington in discussing this project.

Lastly I would like to extend thanks to my family, friends, and fraternity brothers. My families support throughout the duration of this work was truly appreciated. Thanks Mom, Dad, Craig and Jason. Thanks as well to Praveen Sharma, Alexandru Barbu, and the rest of the students in Petroleum and Natural Gas Engineering for helpful suggestions and comments. Furthermore, thanks to my fraternity brothers of the Alpha Delta chapter of Kappa Sigma Fraternity for their support over the past 2 years, A.E.K.Δ.B.

Introduction

Geologists have invoked fault zones as both migration pathways and seals (Figure 1). For example Smith (1966) proposed that hydrocarbons are trapped within sands juxtaposed against low permeability fault zones. Schowalter (1979) suggested that the capillary properties of sealing material could be used to predict the hydrocarbon column height of charged sands (Figure 1). The sealing nature of faults has been well documented (Antonellini and Aydin, 1994; Knipe, 1992; Smith, 1966) and is considered to be the result of petrophysical differences between host rock and fault zone (Scholz and Anders, 1993; Antonellini and Aydin, 1994; Pittman, 1981; Knipe, 1992). The differences in petrophysical properties such as permeability, porosity, sorting, and capillary pressure between fault zones and neighboring reservoirs are believed to be the result of one or more physical processes associated with the deformation that occurs in fault zones.

Pittman (1981) proposed that cataclasis or crushing of rocks in and around fault zones resulted in lower porosity and permeability in the fault relative to the host rock from which it was derived. He further proposed that the grain size sorting of the fault zone was poor relative to the grain size sorting of the host rock, resulting in tighter pore throats and higher capillary entry pressures (Smith (1966) defines capillary entry pressure as the minimum pressure needed to form an interconnected hydrocarbon filament through the pore throats of a rock). Bouvier (1989) suggests that significant reductions in permeability and porosity within the fault zone relative to nearby reservoirs is caused by a process known as clay smear. Clay smear occurs in regions of interbedded shales and sandstones that have undergone deformation due to faulting. Significant faulting can drag large amounts of clay into the fault zone causing a reduction in both permeability and porosity.

Reservoir Sand

Column height
(h) of trapped
hydrocarbons

h
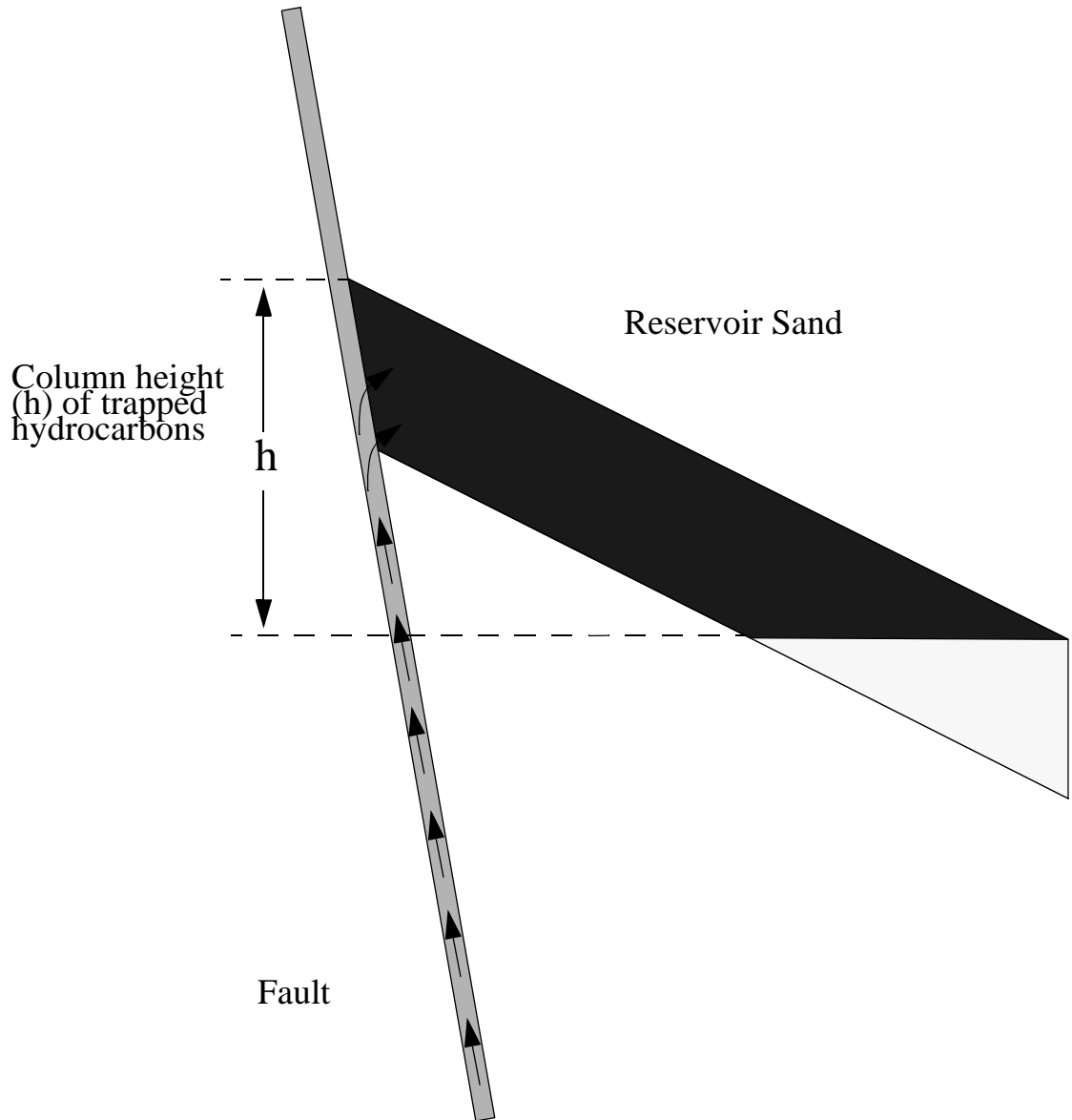
Fault

Figure 1. Conceptual model of a fault zone behaving as both a conduit for migration and
a seal for entrapment of hydrocarbons.

Work by Antonellini and Aydin (1994) shows that these decreases in permeability and porosity between fault rocks and host rocks are about three orders of magnitude and one order of magnitude, respectively. Knipe (1992) suggested that significant reductions in permeability may be obtained without reductions in porosity through a process called Òwash sealÓ. This process reorganizes the clay minerals in the pore throats causing an effective seal at the borders of a fault zone (Knipe, 1992). Hippler (1993) has attributed fault seals to cement deposition in the pore throats of fault zones.

Yet these same faults are often also interpreted to be low permeability migration pathways (Hippler, 1993; Knipe, 1992; Forster et al., 1993). Hippler (1993) suggested that in brecciated regions of fault zones, hydrocarbon staining provided evidence of hydrocarbon migration. Knipe (1992) suggested that migration along fault zones occurs, but that the migration is both localized and episodic.

Thus, there is an apparent contradiction or paradox where faults must both transport and trap hydrocarbons. We use two-phase hydrodynamic modelling to simulate the migration of hydrocarbons through a fault zone and the infilling of adjacent reservoirs. We first present an analytical model of steady state flow through a fault zone and the resultant saturations and column heights. We next simulate the time dependant charging of a fault zone and the resultant infilling of adjacent reservoir sands using a numerical model.

In our analytical model we show that column height is a function of the saturation in the fault zone which is dependent on the rate of charge of hydrocarbons. This result extends the static methodology proposed by Showalter (1979) and shows that column height is a dynamic function of the charge history. In our numerical models we show that the geometry of the reservoir is a critical control in predicting whether reservoir sands will

be fully charged. If the sands are not connected to a large aquifer, hydrocarbons may not

fully charge the sands. We also illustrate the manner by which multiple sands are filled

with hydrocarbons and how the rock properties of the fault zone will control hydrocarbon

migration.

Steady State Flow in a Fault Zone

We first consider the case of one-dimensional steady-state incompressible flow in an isolated fault zone (Figure 2). We assume fluid flow is governed by DarcyÕs Law:

$$Q_o = \frac{k_{ro}kA\,\Delta\Phi_o}{\mu_o}\frac{1}{L} \tag{1}$$

where Q_o is the volumetric oil flow rate from the source rock, k_{ro} is the relative permeability to oil, k is the intrinsic permeability of the rock, A is the cross sectional area of the fault zone normal to flow, μ_o is the oil viscosity, Φ_o is the oil potential, and L is the length of the fault zone. We further assume that the oil injected into the system is dead (i.e. contains no dissolved gas). Assuming the transport of oil up through the fault is driven by gravity, the driving force, $\Delta\Phi_o/L$, (otherwise known as the buoyancy gradient) can be written as:

$$\frac{\Delta\Phi_o}{L} = \Delta\rho g\cos\theta \tag{2}$$

where $\Delta\rho$ is the density difference between oil and water, g is the gravitational acceleration, and θ is the angle from vertical of the fault zone.

The relative permeability of the system to oil and water is modeled with CoreyÕs approximation,

$$k_{rw} = (S_w^{\,a})^4 \tag{3}$$

$$k_{ro} = 1\,Ð\,2S_w^{\,a} + 2(S_w^{\,a})^2 Ð(S_w^{\,a})^4 \tag{4}$$

where

$$S_w^{\,a} = \frac{S_w\,Ð\,S_{wirr}}{1\,Ð\,S_{wirr}} \tag{5}$$

where S_{wirr} is the irreducible water saturation, and S_w is the water saturation (Ertekin,
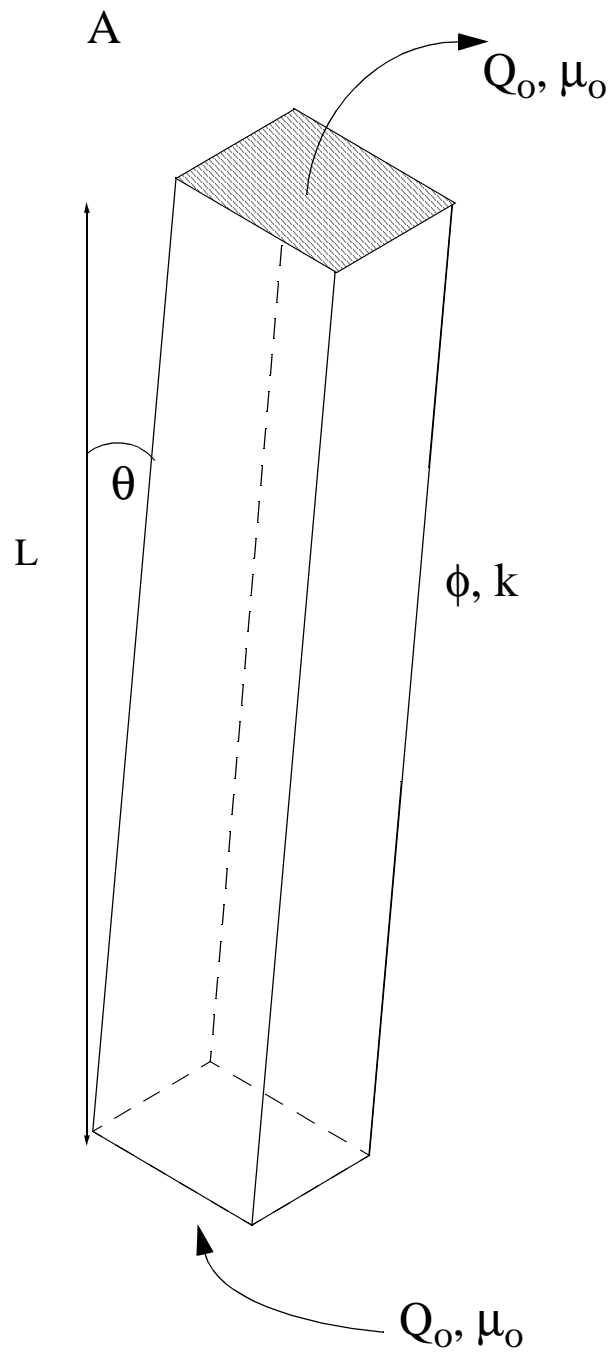
Figure 2.   Physical description of the analytical system (fault zone).

1993). Figure 3 is a graphical representation of CoreyÕs approximation for water and oil relative permeability.

Substituting Equations 2 and 4 into Equation 1, the following relationship between oil flux and fault zone saturation is obtained:

$$\frac{Q_o}{A} = \frac{[1 Ð 2S_w{}^a + 2(S_w{}^a)^2 Ð (S_w{}^a)^4]k}{\mu_o} \Delta \rho g \cos \theta \tag{6}$$

Equation 6 states, that for specific rock and fluid properties, the fault zone saturation is a function of the flux. This is illustrated in Figure 4 for the properties shown in Table 1.

In this paper we will be considering several specific simulations where the fault is considered to have a rectangular cross-sectional area of 334.5 m^2 (3600 ft.^{2}) and a porosity of 5.0%. Both a low permeability fault and a high permeability fault are considered with permeabilities of 0.01 and 0.10 millidarcies, respectively. In our analysis, the viscosities and densities of oil and water are assumed constant (Table 1).

Table 1: Parameters for the Fault Zone

Fault Cross Section	334.5 m^2
Fault Porosity	5.0 %
High Perm Fault Permeability	0.10 millidarcies
Low Perm Fault Permeability	0.01 millidarcies
Oil viscosity	3.519*10^{-4} Pa*s
Water Viscosity	1.838*10^{-4} Pa*s
Oil Density	849.8 kg/m^3
Water Density	999.9 kg/m^3
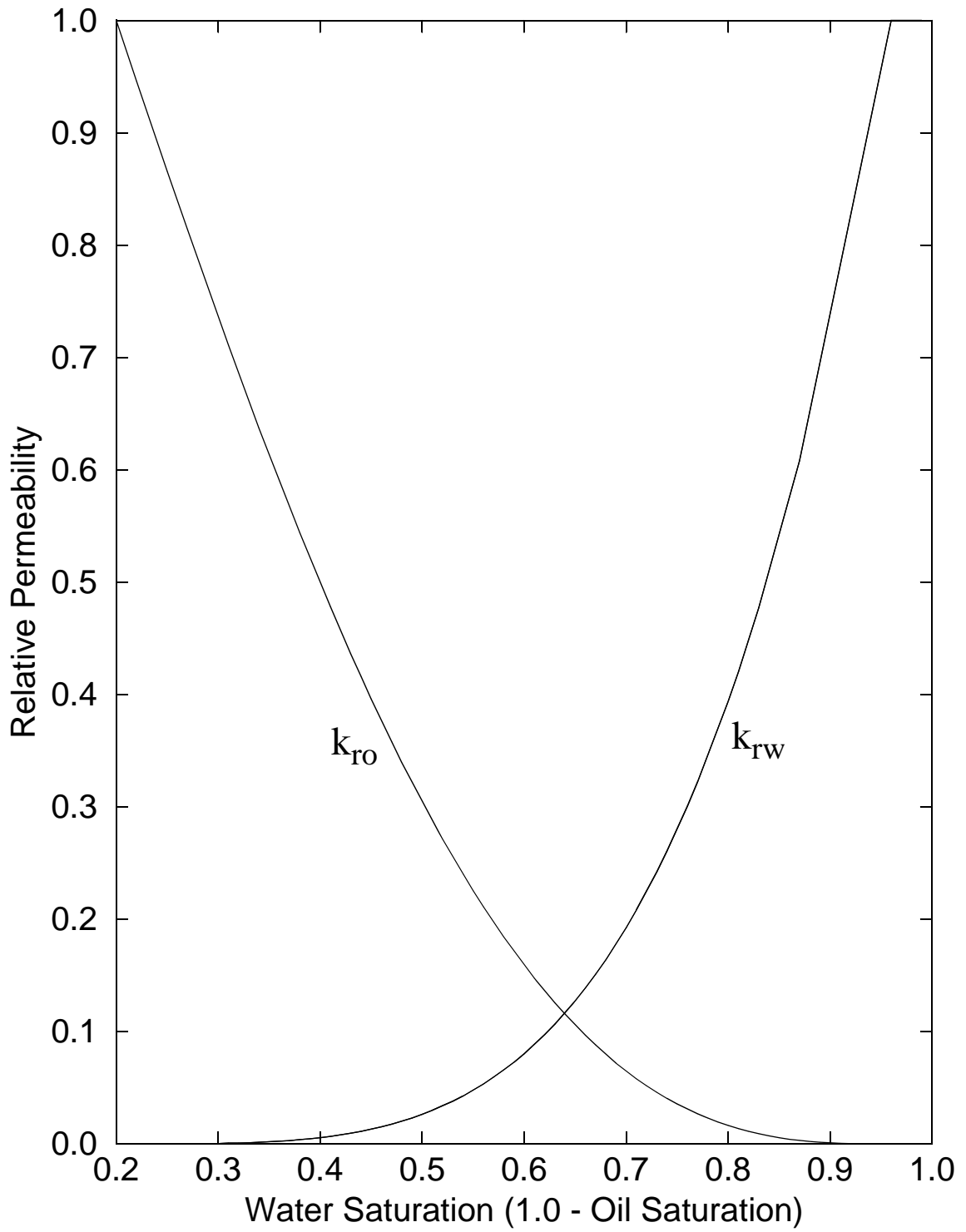
Figure 3. CoreyÕs approximation of relative permeability in the fault zone and reservoir as a function of water saturation.
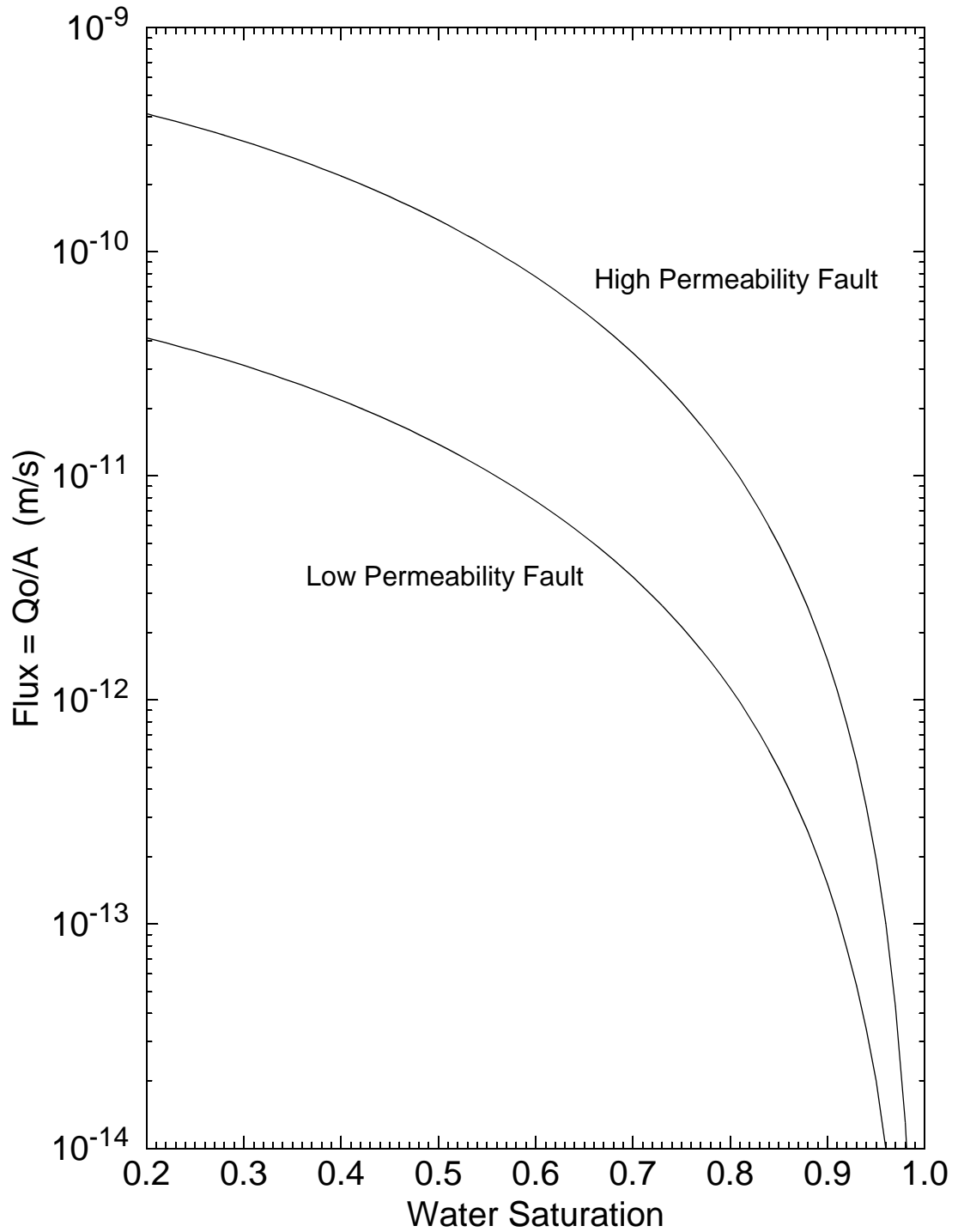
Figure 4.   Flux versus water saturation in the high and low permeability fault zones. Solution of Equation 6 from water saturation of 0.2 to 1.0 assuming CoreyÕs approximation for the relative permeability data (Figure 3).

We will model a flux of $1.13*10^{-11}$ m/s. We solve Equation 6 for the above conditions and find a steady-state fault oil saturation of 46% and 20% for the low permeability (0.01 millidarcies) and high permeability (0.1 millidarcies) models, respectively. Figure 4 illustrates a range of solutions for these two fault permeabilities. Note the curves in Figure 4 are just the relative permeability to oil curves scaled by the constant $k\Delta\rho g\cos\theta/\mu_o$ (see Equation 6).

Column Height in Adjacent Sands During Steady-State Flow

We next consider steady-state flow in a fault with an adjacent reservoir abutted against the fault (Figure 5). The reservoir and the fault zone are assumed to have different petrophysical properties. As discussed in the previous section, during steady-state flow the fault saturation is constant. If a reservoir is abutted against the fault (Figure 5), it will fill with hydrocarbons (from the fault zone) until the capillary pressure at the top of the reservoir is equal to the capillary pressure within the fault zone.

ThomeerÕs relationship (Jorden and Campell, 1984) is used to model the capillary pressure in the fault and reservoir:

$$P_c = e^{\left(\left[\log P_d Ð\left(\dfrac{G}{\log\left(\frac{S_O}{1 Ð S_{wirr}}\right)}\right)\right]\right)} \tag{7}$$

where P_c is the capillary pressure, P_d is the capillary entry pressure, G is the pore geometrical factor and S_o is the oil saturation. Equation 7 is used to define the capillary pressure curves for the 0.1 millidarcy fault and a reservoir with a horizontal permeability of 1.0 millidarcies, a vertical permeability of 0.1 millidarcies, and a porosity of 20%. (Figure 6). The parameters specifically used to define the capillary pressure curves for the reservoir and the high permeability fault zone are shown in Table 2.

Table 2: Parameters for ThomeerÕs Relationship

Variable	Reservoir	High Permeability Fault Zone
Pd	5.0 psi	10.0 psi
G	0.5	0.1
S_{wirr}	0.20	0.20

Q_o, μ_o

A

ϕ_{fault}
k_{fault}

θ

L

h

ϕ_{sand}

Q_o, μ_o
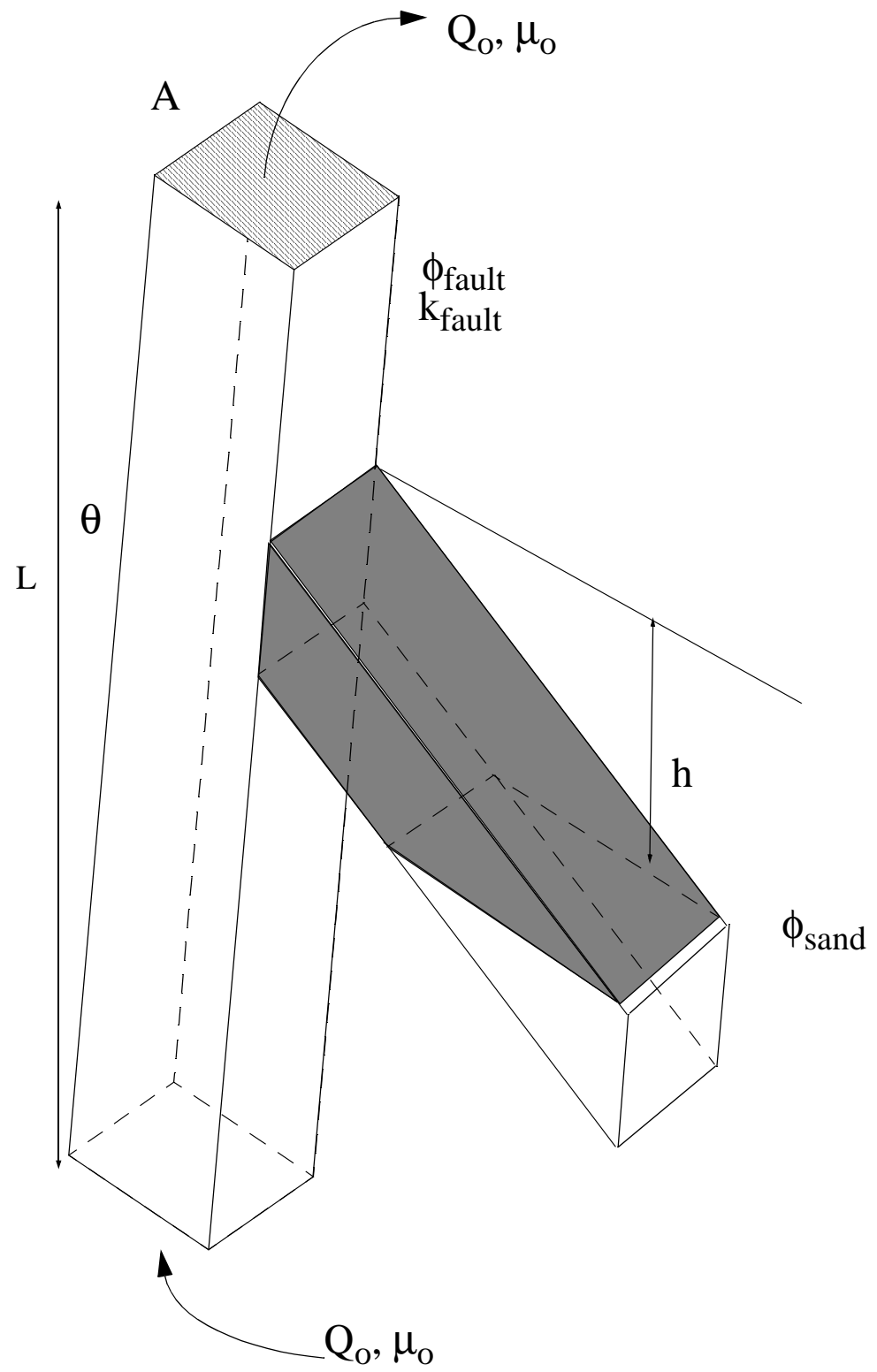
Figure 5.   Physical description of analytical system with sand and hydrocarbons.
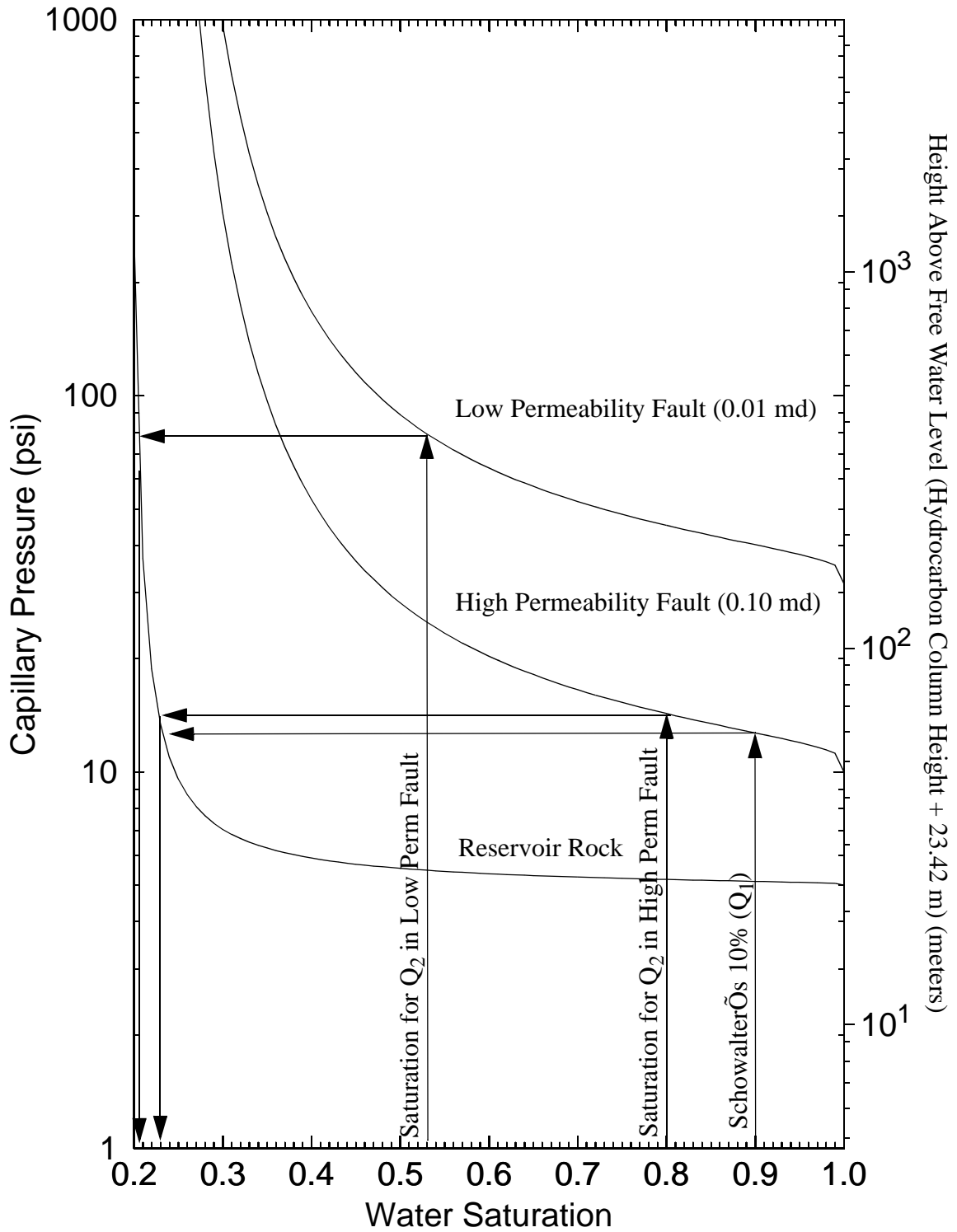
Figure 6.   Capillary pressure relationships for the sand and the two faults illustrating the relationship between fault zone saturation and reservoir saturation. At a steady state the capillary pressure in the reservoir is equal to that in the fault.

We use the Leverett-J function (Amyx et al., 1960) to scale the capillary pressure of the lower permeability fault from the capillary pressure of the higher permeability fault:

$$J(S_w) = \frac{P_c(S_w)}{\sigma} \left(\frac{k}{\phi}\right)^{\frac{1}{2}} \qquad (8)$$

where $J(S_w)$ is the J function, σ is the interfacial tension between the oil and water phases (20 dynes/cm) and ϕ is the porosity (5.0% for the fault). Equation 8 allows scaling of capillary pressure relationships to be a function of both permeability and porosity. Figure 6 illustrates the resulting capillary pressure curves for the reservoir, the low permeability fault, and the high permeability fault.

As discussed in the previous section, a steady state flow rate in the fault zone results in a constant saturation of the fault zone. At steady-state, both the oil and water pressures will tend to equalize across the fault-reservoir interface. Therefore the capillary pressure in the reservoir will approach the capillary pressure of the fault. The two cases from the previous section are examined below. For the low permeability fault zone, the steady-state oil saturation of the fault is 47%. At this saturation the capillary pressure in the fault is 79 psi ($5.44*10^5$ N/m^2). Since the capillary pressure in the reservoir will be the same, the oil saturation at the top of the reservoir should reach 79%. For the high permeability fault zone, the steady-state oil saturation of the fault is 20%. The corresponding capillary pressure is 14 psi ($9.66*10^4$ N/m^2) which neccessitates an oil saturation of 77% at the top of the reservoir.

The final stage is to relate the capillary pressure in the reservoir to the column height present. Capillary pressure is defined as the difference between the oil and water pres-

sures:

$$P_c = P_o Ð P_w \qquad (9)$$

where P_o is the oil pressure and P_w is the water pressure. At the free water level the oil and

water pressures are equal, P_c=0. Above the free water level, fluid pressures are propor-

tional to h, the height above the free water level:

$$P_o = P_{FWL} Ð \rho_o gh \qquad (10)$$

$$P_w = P_{FWL} Ð \rho_w gh \qquad (11)$$

Substituting Equations 10 and 11 into Equation 9 and solving for h yields:

$$h = \frac{P_c}{(\rho_w Ð \rho_o)g} \qquad (12)$$

We use Equation 12 and our capillary pressure relationship (Figure 6) to calculate the

oil column height versus fault zone saturation in Figure 6 (opposite axis). Note that the

actual hydrocarbon column height will be less than h if P_c at $S_w = 1.0$ is greater than zero

for the reservoir (as illustrated in Figure 6). In this case the actual hydrocarbon column

height, h_{oil}, is:

$$h_{oil} = \frac{P_c(\text{at top of sand}) Ð P_c(\text{at } S_w = 1.0)}{(\rho_w Ð \rho_o)g} \qquad (13)$$

Given this approach, we calculate steady-state column heights of 347 meters and 44

meters (1140 feet and 143 feet) for the low and high permeability cases, respectively.

A similar approach was used by Schowalter (1976) to predict column height as a func-

tion of capillary pressures of the seal rock. We emphasize, however, one important distinc-

tion, in SchowalterÕs model column height is dependent only on the capillary pressure

curveÕs Òbreak throughÓ point. At this point (typically ~10% oil saturation) the buoyant

forces of the hydrocarbon column are large and the seal will leak (Figure 6). Work per-

formed by Katz and Thompson (1986) suggests that the leaking potential of a seal may be

predicted by determining the inflection point of the capillary pressure curve. The inflec-

tion point of the capillary pressure curve is considered to be the minimum saturation

needed to form a continuous stream of hydrocarbons across the zone of interest, allowing

hydrocarbon migration. Our model is different than both of these models because the cap-

illary pressure within the fault zone is a function of the saturation which is ultimately a

function of the flux into the fault. SchowalterÕs model does not consider the seal as a

potential migration pathway. Our model does and this allows for dynamic hydrocarbon

column heights that are a function of hydrocarbon flux into the fault.

Extending this methodology, we propose a method for determining the approximate

time needed to fill the reservoir to steady state hydrocarbon column height. We assume

that all oil injected into the fault enters the reservoir until a steady state hydrocarbon col-

umn height is achieved. In addition, we neglect the pore volume of the fault in our calcula-

tions. From Figure 6 we may determine the analytical steady state oil saturation

throughout the reservoir as a function of height. Using this analytical oil saturation, we

may determine an average saturation throughout the reservoir. Once we have determined

this average saturation, we calculate the volume of oil needed to fill the reservoir to the

predicted hydrocarbon column height. Simply dividing the volume of oil needed by the

flowrate of oil into the fault will approximate the time required to fill the reservoir.

We illustrate this method with an example. From the previous section, we predicted

that a low permeability (0.01 millidarcies) fault zone and a flux of $1.13*10^{-11}$ m/s would

produce a hydrocarbon column height of 347 meters. Equation 14 is the equation used to

predict the average saturation in the reservoir:

$$Average \ S_O \ = \ \frac{\int_0^{h_{oil}} S_O(h) \ dh}{\int_0^{h_{oil}} dh} \tag{14}$$

where h_{oil}, is the height of the steady state oil column. For example, we numerically inte-

grate oil saturation versus column height of the reservoir (Figure 6) from 0 to 347 meters,

divide through by our column height and find the average oil saturation to be 78.6%

throughout the reservoir. We then calculate the pore volume of rock that will be saturated

with oil, multiply this by the average oil saturation of 78.6%, and divide by the flowrate to

obtain a fill time of 5.8 million years.

Numerical Simulations

We now consider the application of these principals to numerical simulations. Using the ECLIPSE 100 reservoir simulation package developed by Intera, we model the time dependent hydrodynamic flow of oil through a fault zone and into adjacent reservoirs. In all simulations we specify a constant pressure boundary at the top of the fault of 2000 psi ($1.38*10^7$ N/m^2) and a constant flowrate at the bottom of the fault. Oil is injected at a rate of $3.77*10^{-9}$ m^3/s ($2.05*10^{-3}$ Bbls/Day) for all but one of the simulations. We present six simulations investigating the sensitivity of results to fault rock properties, flux into the fault zone, and reservoir geometry.

The two geometries presented are illustrated in Figure 7. Figure 8a represents the grid used for simulating infinite reservoirs (Figure 7a) and Figure 8b represents the grid used for simulating finite reservoirs (Figure 7b). The grid blocks connecting the periphery of the reservoir to the fault zone (Figure 8a) assure a hydrostatic pressure boundary at the edge of the simulated infinite reservoir. This geometry is interpreted geologically, as a large regional reservoir (Figure 7a). The lack of these grid blocks (Figure 8b) create a no-flow boundary at the periphery of the reservoir which may be interpreted geologically as a stratigraphic pinch out (Figure 7b), a faulted section with little or no permeability, or a localized sand lens.

a) Constant Pressure
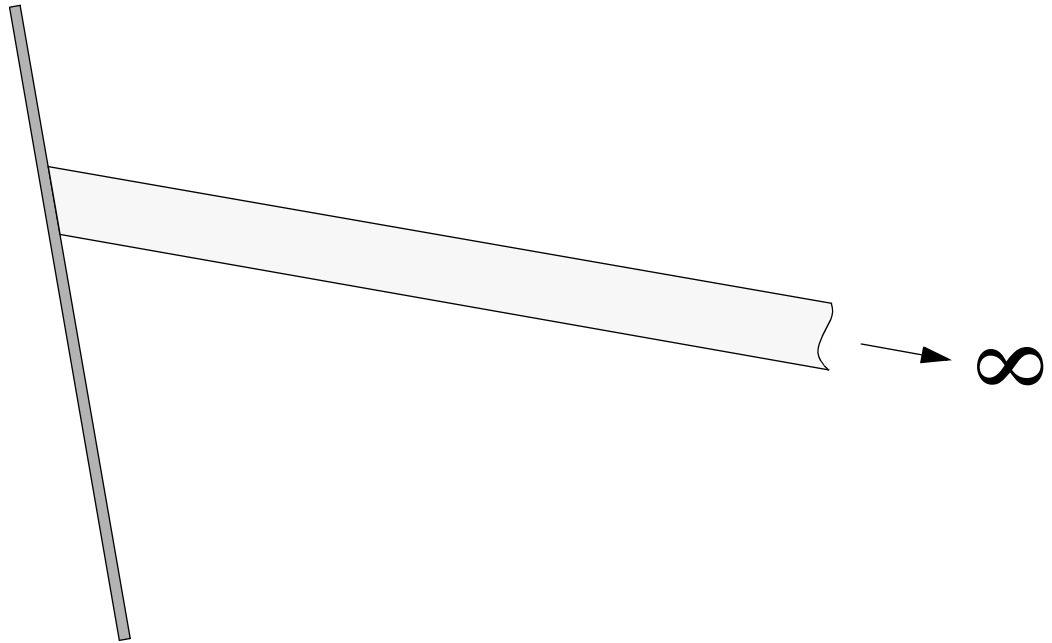
b) No-Flow
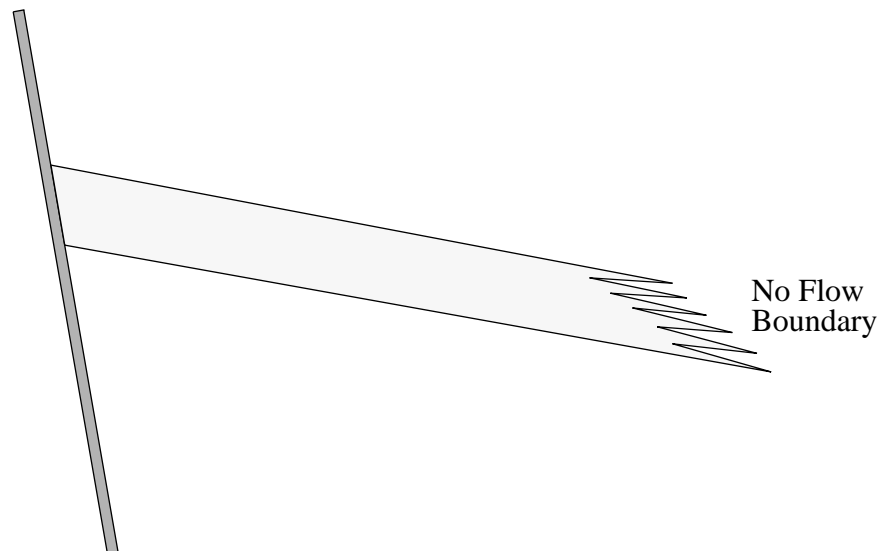
No Flow
Boundary

Figure 7.   Conceptual models for simulations. a) A regional and infinite reservoir. b) A
local and finite reservoir.

a) Constant Pressure

Grid blocks connecting
periphery of the reservoir
to the fault
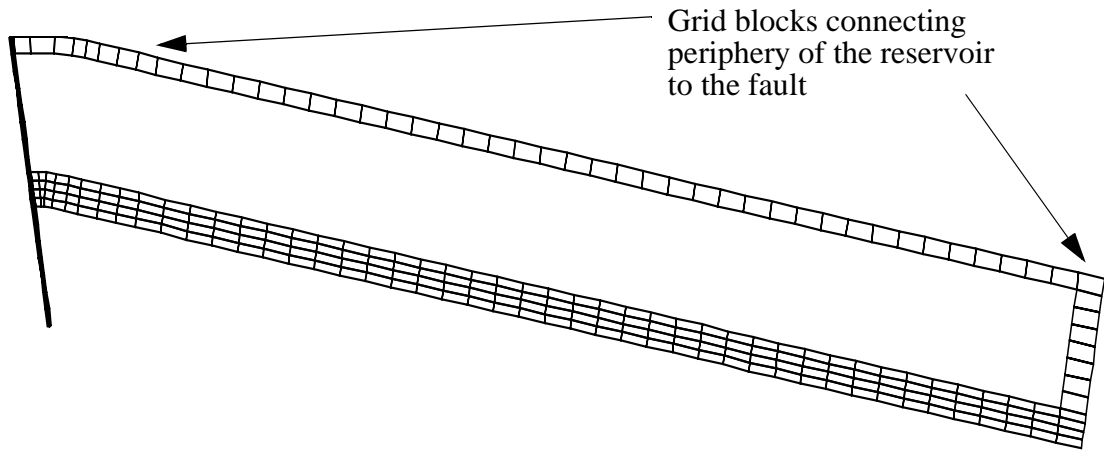
b) No-Flow
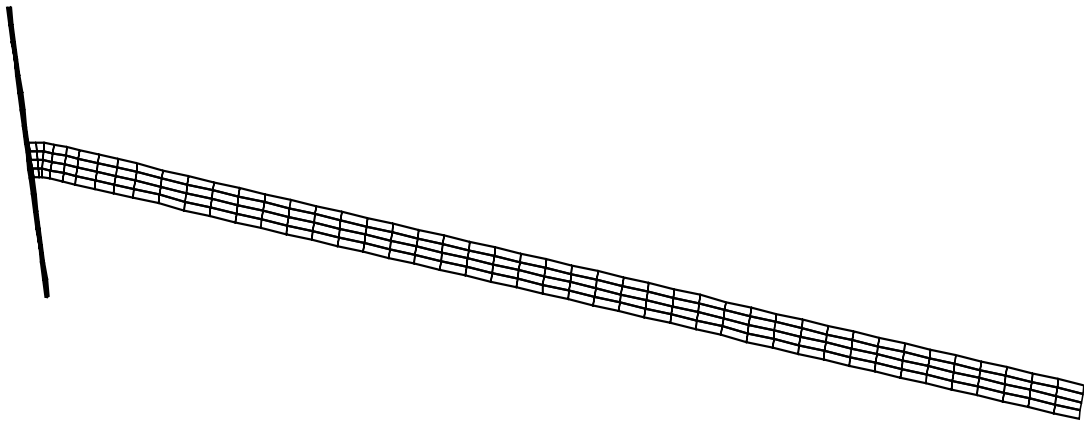
Figure 8.   Model geometry for the numerical simulations. a) Infinite reservoir b) Finite
reservoir

RUN_1: High Permeability Fault and Infinite Reservoir

The first numerical simulation we present illustrates SchowalterÕs static methodology. We simulate a high permeability (0.10 millidarcies), isotropic, homogeneous fault zone connected to a relatively high permeability (1.0 millidarcies horizontal direction and 0.10 millidarcies vertical direction), anisotropic, homogeneous infinite reservoir (Figure 7a).

The capillary pressure curves for the fault zone and the reservoir are taken from the example mentioned before (Figure 6). The relative permeability curves for both the fault and the reservoir are shown in Figure 3. The flux of oil is $1.13*10^{-12}$ m/s and dictates a steady-state oil saturation of approximately 10% in the fault zone (Equation 6). Analytically, an oil saturation of 10% in the fault zone will charge the reservoir with 35 meters of oil (Figure 6) in 3.4 million years.

The numerical simulation generates an oil column approximately 34 meters high in the reservoir shortly after 3 million years (Figure 9), at which point steady state is reached. The difference in oil potential (driving force) from the fault into the sand as a function of time illustrates that initially there is a driving potential of approximately 6 psi from the fault into the sand (Figure 10). As time passes, the difference in oil potential begins to decrease in the first and second blocks of the interface (Figure 10). This equalizing in the first two blocks of the fault-reservoir interface is due to the charging of the reservoir. The remaining potential in the third and fourth blocks of the fault reservoir interface is a function of the height of the hydrocarbon column and the thickness of the reservoir. The reservoir itself is 61 meters thick and a 34 meter oil column does not saturate the full extent of this interface. Therefore, driving potential remains in the third and fourth grid
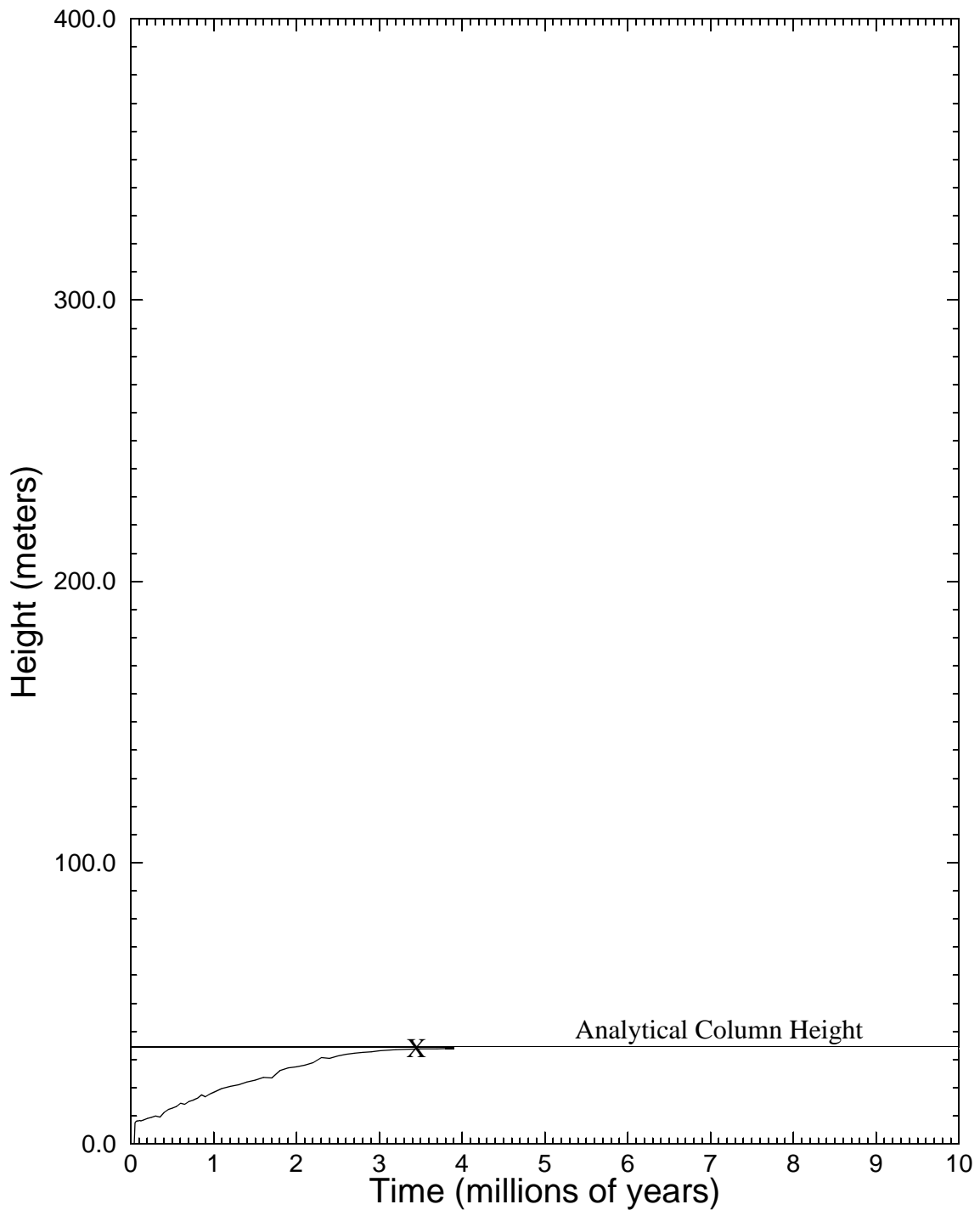
Figure 9. Hydrocarbon column height versus time for the high permeability fault and infinite reservoir simulation used to illustrate SchowalterÕs static methodology (RUN_1). Steady-state height is 34 meters numerically and 35 meters analytically. The X represents the analytically calculated time required to fill the sand to a steady state hydrocarbon column of 35 meters.
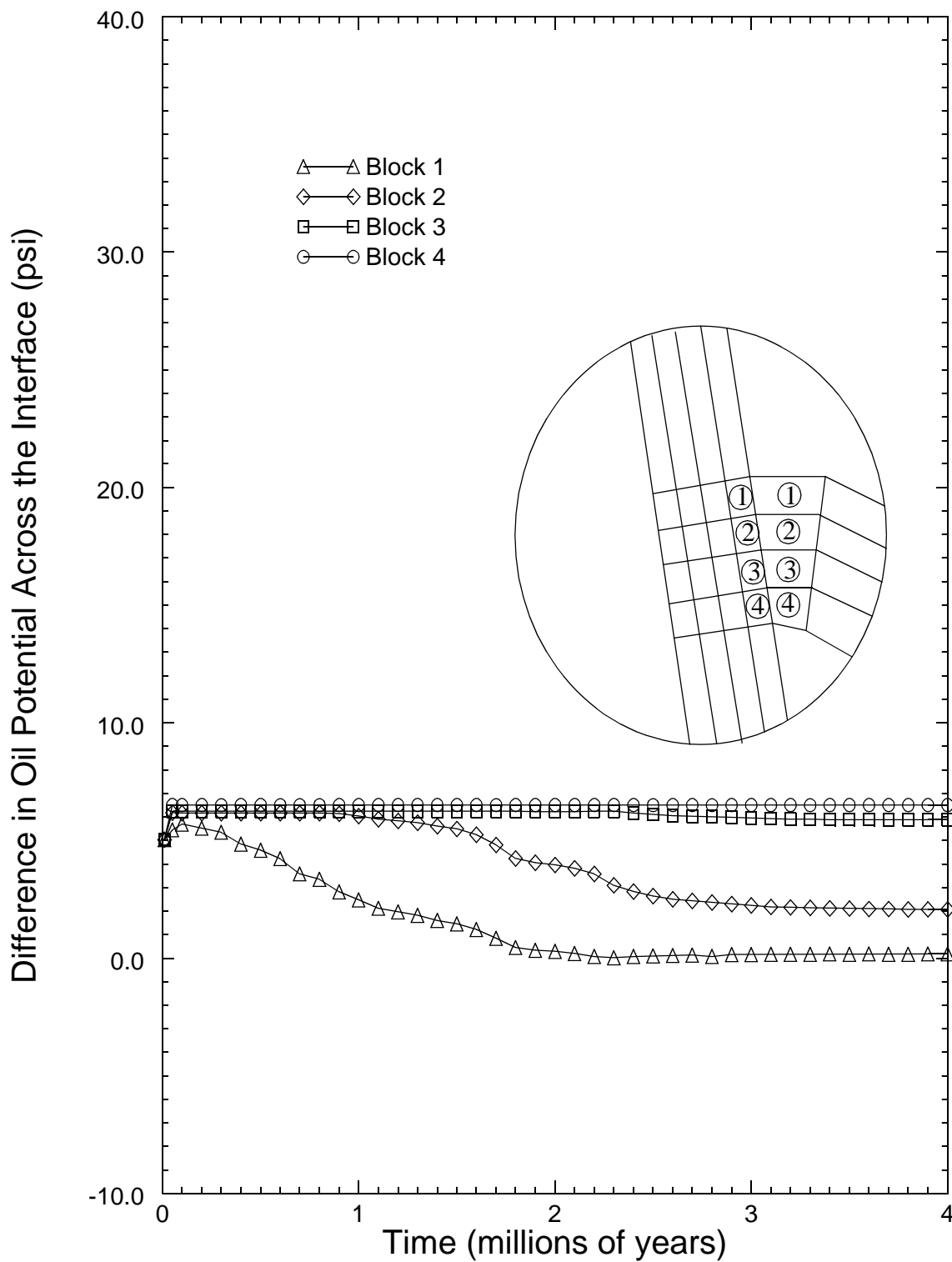
Figure 10. Difference in oil potential through time across the fault-reservoir interface for RUN_1. Values are calculated so that a positive difference in potential represents a driving force from the fault into the reservoir.

blocks. Oil flows into the these grid blocks, rises upwards in the reservoir, breaches the

sealing potential of the fault zone causing the fault to leak maintaining the hydrocarbon

column at 34 meters. The difference in water potential between the reservoir and the fault

zone shows no driving force (Figure 11).

Increased oil saturations cause the water relative permeability to drop in the reservoir

near the reservoir-fault interface (Figure 12). The water relative permeability drops to

nearly zero in the first and second blocks of the reservoir. Furthermore, water relative per-

meability drops to steady-state values of 0.032 and 0.747 for the third and fourth grid

blocks, respectively (Figure 12). Once again, this is attributed to the steady-state oil satu-

ration along the fault-reservoir interface where oil saturations are high in the first and sec-

ond blocks of the reservoir and low in the third and fourth blocks of the reservoir along the

interface (Figures 13 and 14). Figure 13 and Figure 14 are selected time slices of oil satu-

ration versus location.

SchowalterÕs (1979) hypothesis states that the potential of sealing materials, in this

case the fault zone, is a static function of the sealing materialÕs capillary pressure at satu-

rations of ~10% oil. For this example, SchowalterÕs theory predicts that an oil column of

35 meters may be supported by the fault zone. Our next example is intended to show that

the sealing capacity of fault zones acting as conduits for oil migration and seals for oil

accumulation, is not a static function of the capillary pressure at ~10% oil saturation.

Rather, we intend to show that the sealing capacity of faults acting as secondary migration

conduits is a dynamic function of the flux into those fault zones, the saturations that ensue

and the resulting capillary pressures.
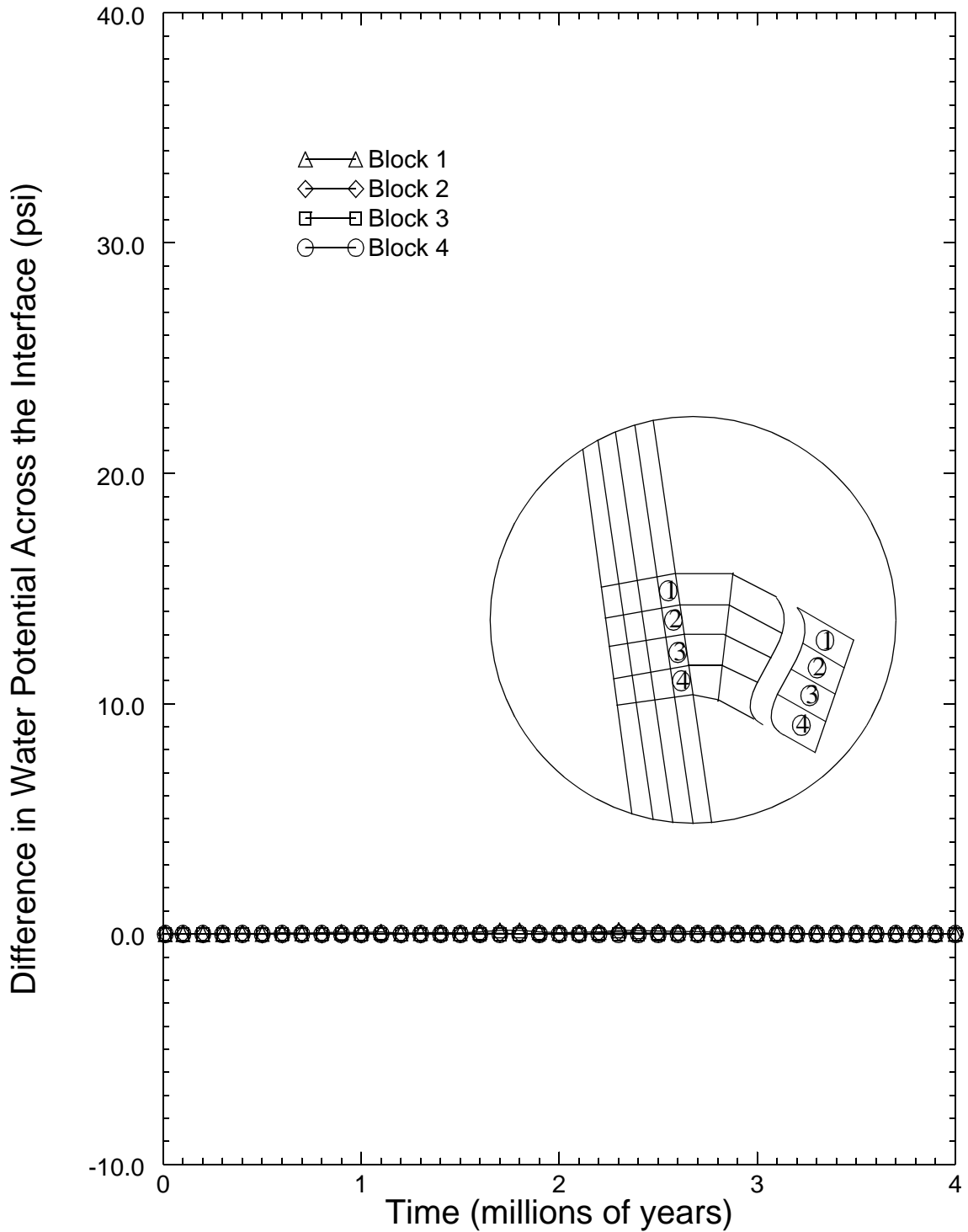
Figure 11. Difference in water potential through time from the outermost block in the
sand to the first block in fault next to the interface for RUN_1. Values are cal-
culated so that a positive difference in potential represents a driving force from
the the reservoir into the fault.
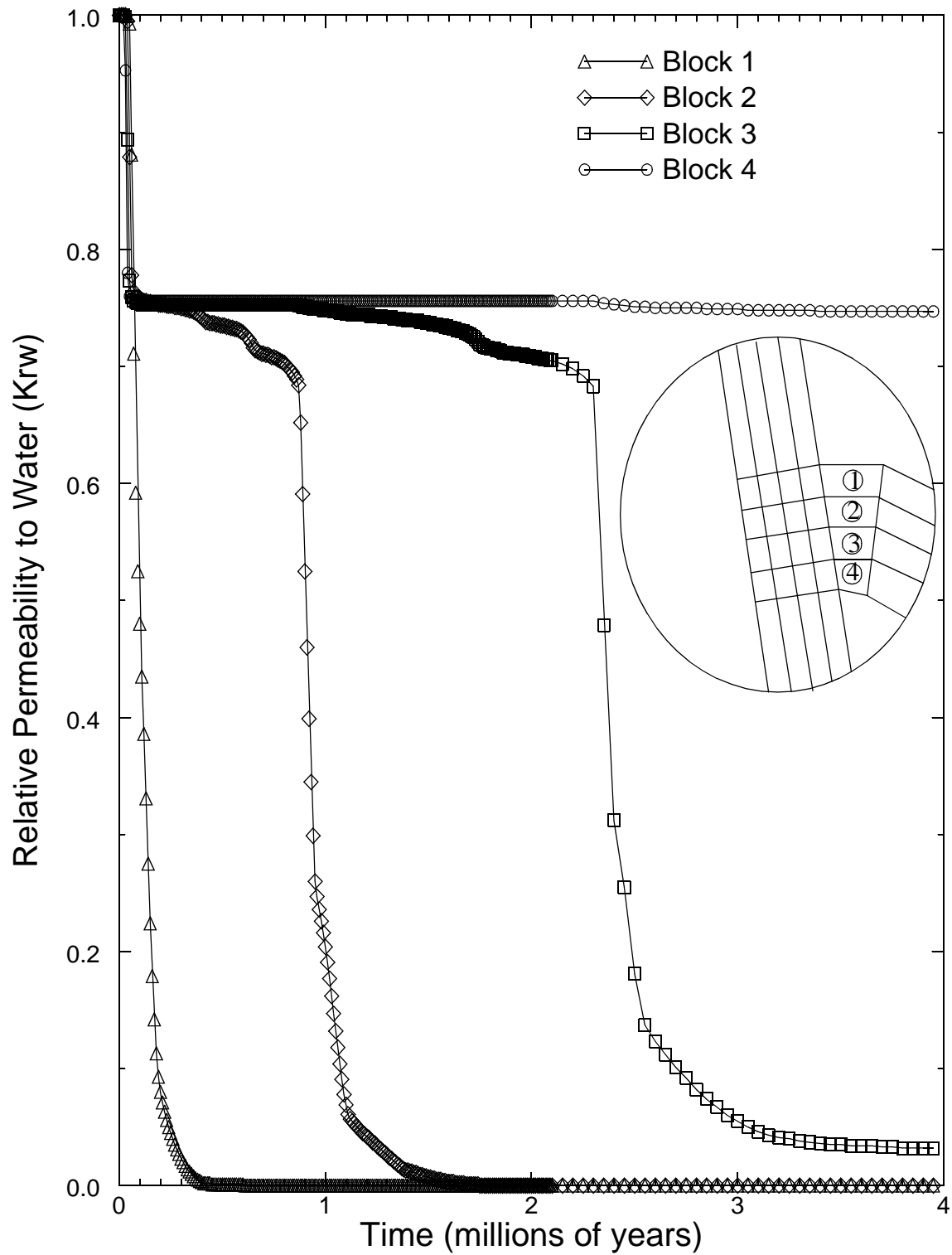
Figure 12. Relative permeability through time of the reservoir grid blocks next to the fault-reservoir interface for RUN_1.

0.25 million years

0.5 million years

1.0 million years

1.5 million years

500 m

0.00   0.25   0.50   0.75   0.80
Oil Saturation
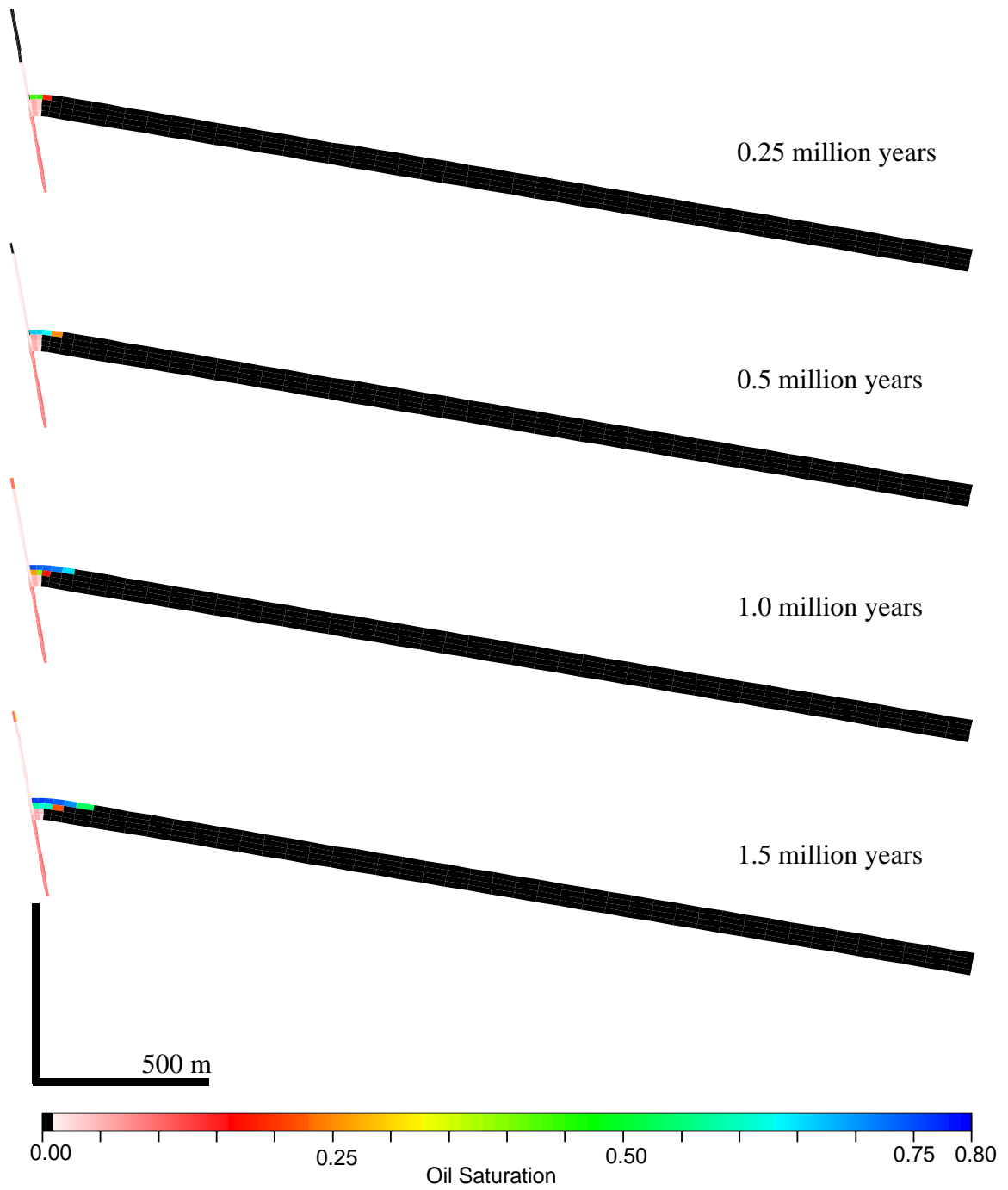
Figure 13. Saturation of oil versus location for RUN_1 at 0.25, 0.50, 1.00 and 1.50 million years.
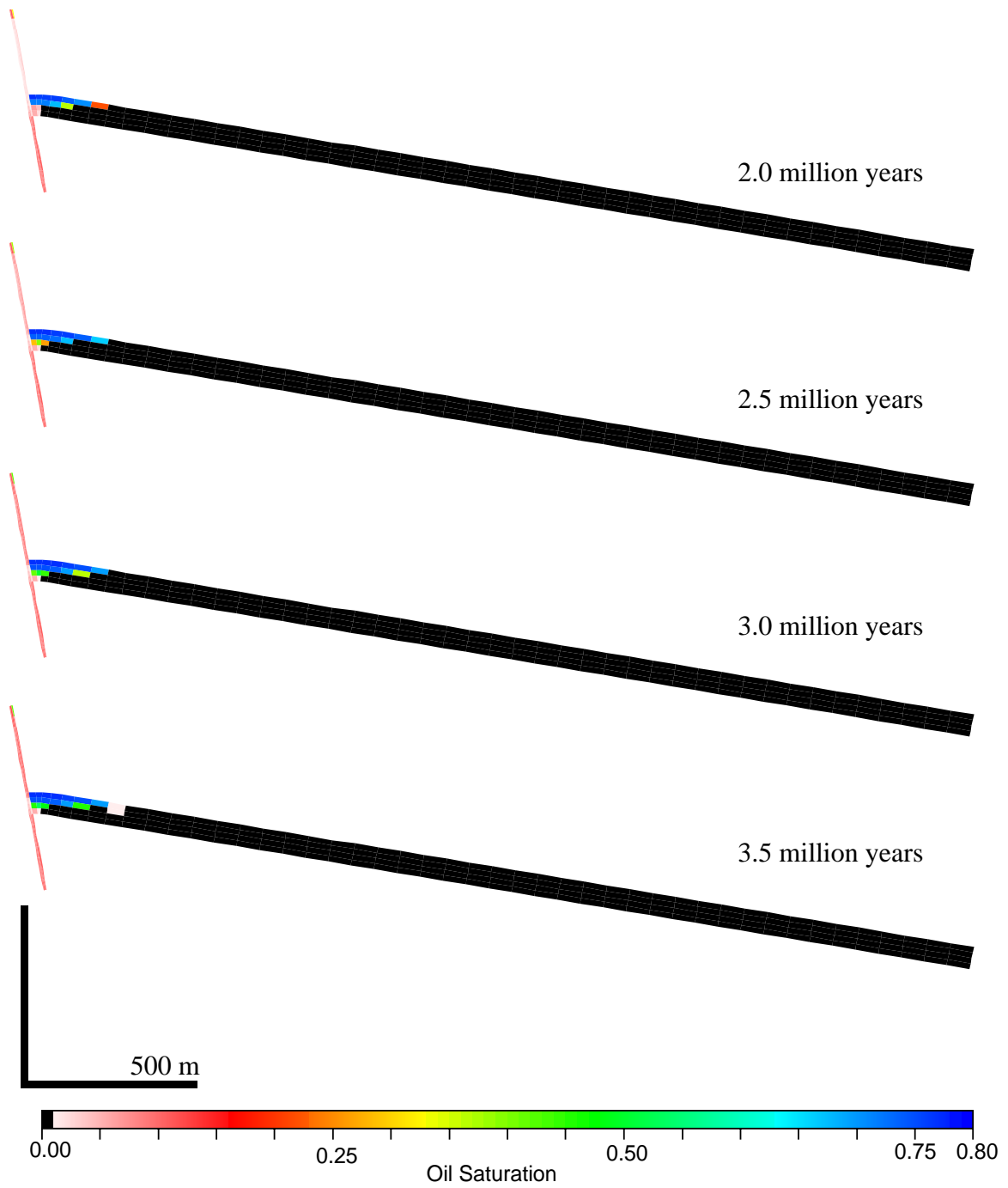
Figure 14. Saturation of oil versus location for RUN_1 at 2.00, 2.50, 3.00 and 3.50 million years.

RUN_2: High Permeability Fault and Infinite Reservoir

The next simulation is identical to the first simulation except the flux rate into the fault is one order of magnitude higher ($1.13*10^{-11}$ m/s). This, in turn, increases the steady-state oil saturation in the fault zone from 10% to 20% oil (Equation 6). Analytically, we predict a hydrocarbon column height of 44 meters (145 feet) (Equation 13) in 0.5 million years.

The results of this simulation show a hydrocarbon column height of 42 meters (138 feet) after 1.0 million years (Figure 15). Figure 16 illustrates the difference in oil potential between the fault and the reservoir through time. Initially, this difference is high in all 4 grid blocks. After 0.6 million years the difference in oil potential drops to nearly zero in the first and second blocks of the reservoir (Figure 16). The difference in potential at the interface for the third and fourth grid blocks, however, does not drop to zero indicating that the oil potential across the interface is not in equilibrium. Oil enters into the third and fourth grid blocks of the reservoir after steady state is reached and rises up in the reservoir and re-enters the fault in the same manner as described for the first simulation.

The relative permeability to oil is high in the reservoir, therefore only a small oil potential is required for the oil to flow back into the fault from the reservoir. Figure 17 illustrates that water has essentially no driving potential from the reservoir into the fault. This lack of driving potential in water is due to the lack of hydrocarbon column height. The hydrocarbon column height is small relative to the thickness of the reservoir and water may freely escape from the sand to the fault.

The relative permeability of water in the reservoir blocks next to the interface is shown in Figure 18. We notice that the relative permeability of the fourth grid block does not approach zero, but achieves a steady-state value of about 0.45. Since the hydrocarbon
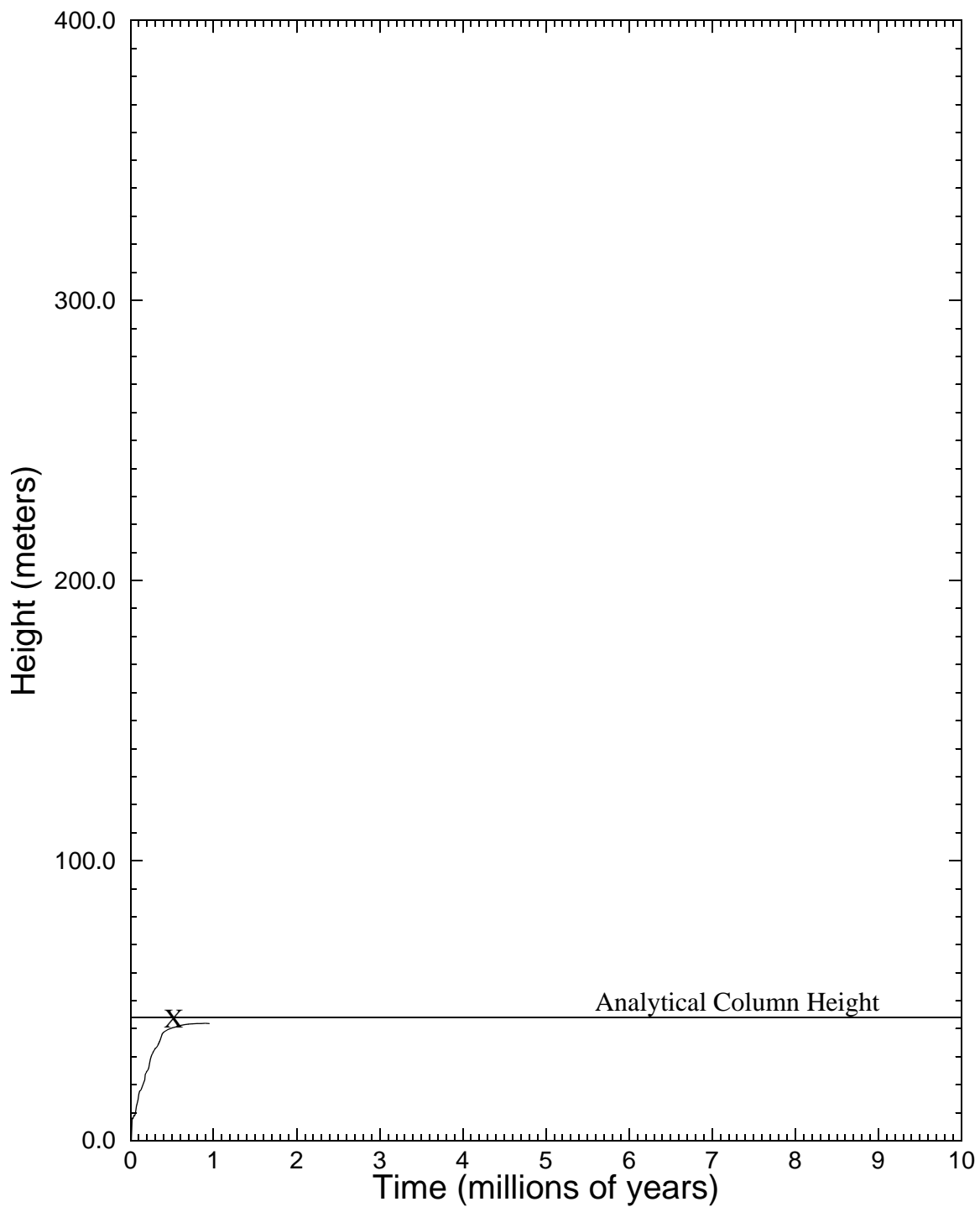
Figure 15. Hydrocarbon column height versus time for the high permeability, infinite res-
ervoir simulation (RUN_2). Steady-state height is 42 meters numerically and
44 meters analytically. The X represents the analytically calculated time
required to fill the sand to a steady state hydrocarbon column of 44 meters.
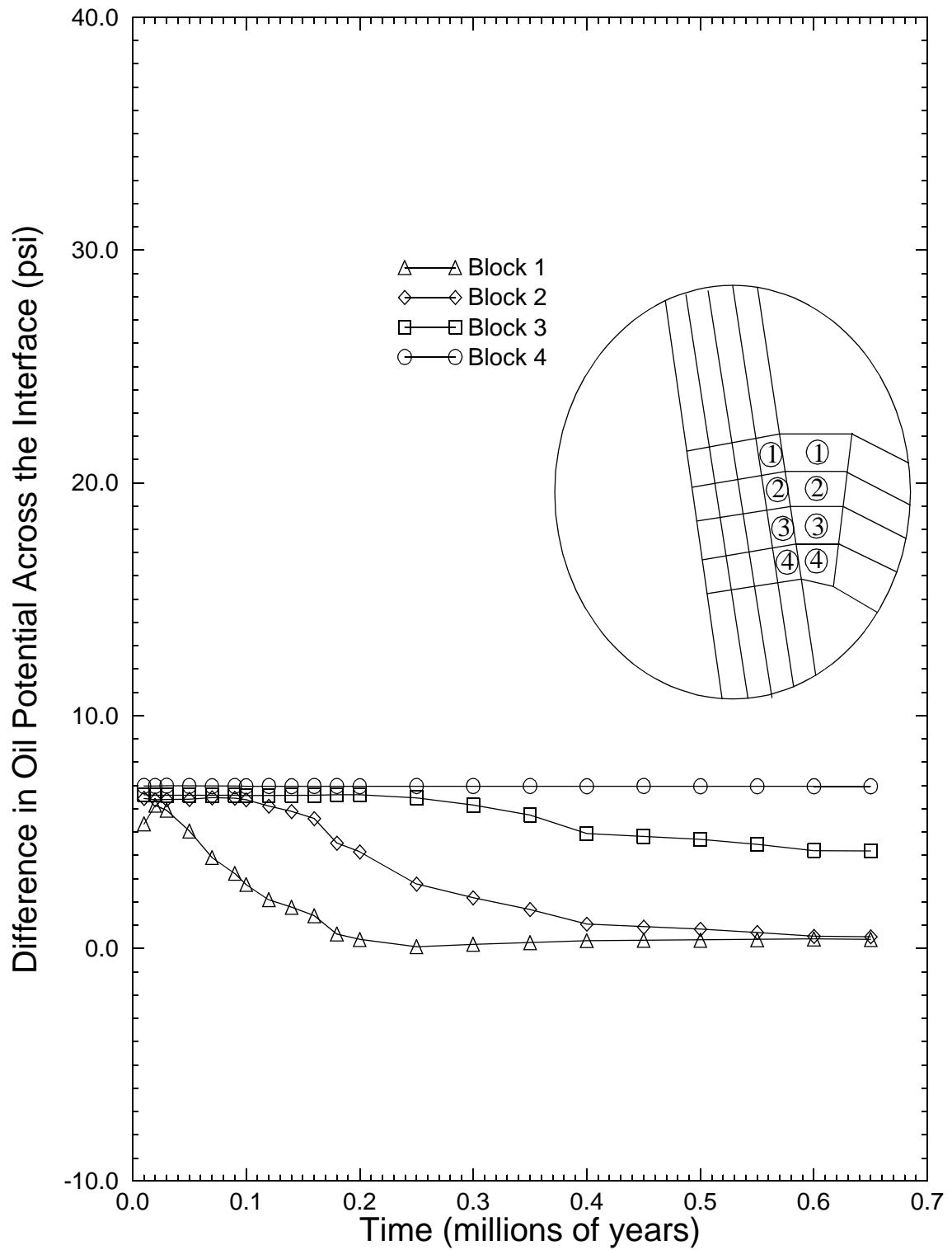
Figure 16. Difference in oil potential through time across the fault-reservoir interface for RUN_2. Values are calculated so that a positive difference in potential represents a driving force from the fault into the reservoir.
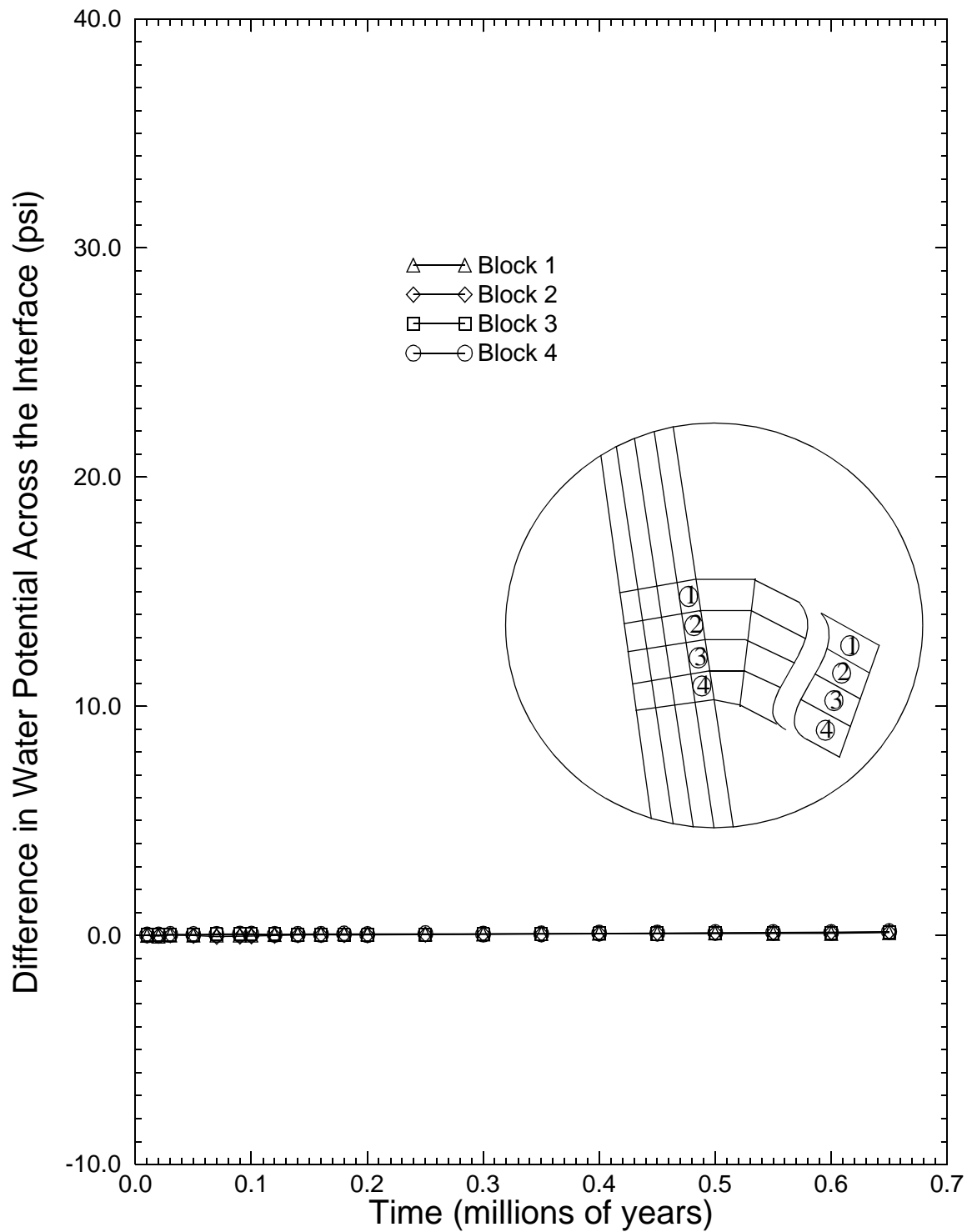
Figure 17. Difference in water potential through time from the outermost block in the sand to the first block in fault next to the interface for RUN_2. Values are calculated so that a positive difference in potential represents a driving force from the the reservoir into the fault.
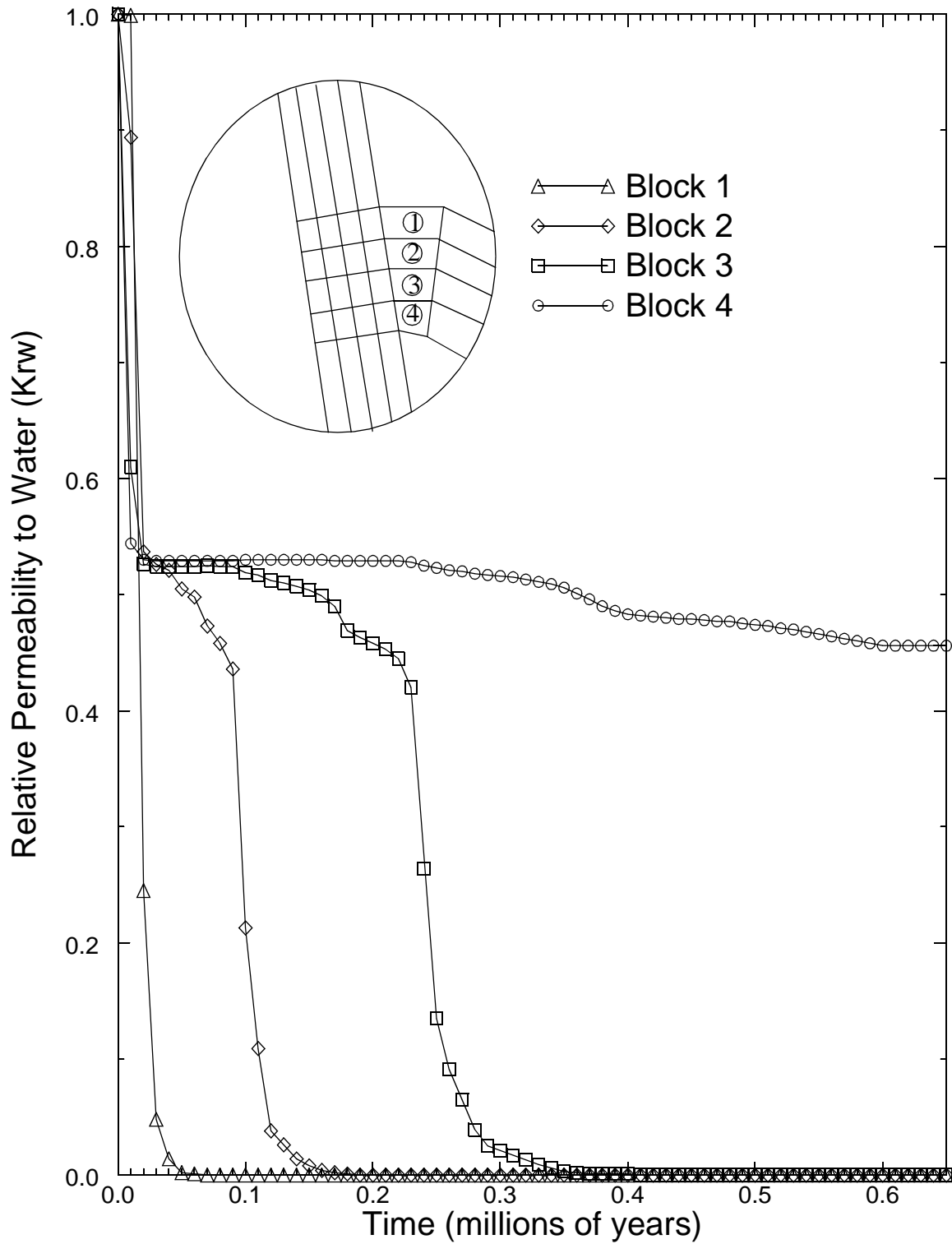
Figure 18. Relative permeability through time of the reservoir grid blocks next to the fault-reservoir interface for RUN_2.

column is only 42 meters (138 feet), the oil saturation remains relatively low in the fourth grid block. Therefore, we do not see a drop in water relative permeability to zero in this block. Figure 19 is selected time slices of oil saturation versus location.
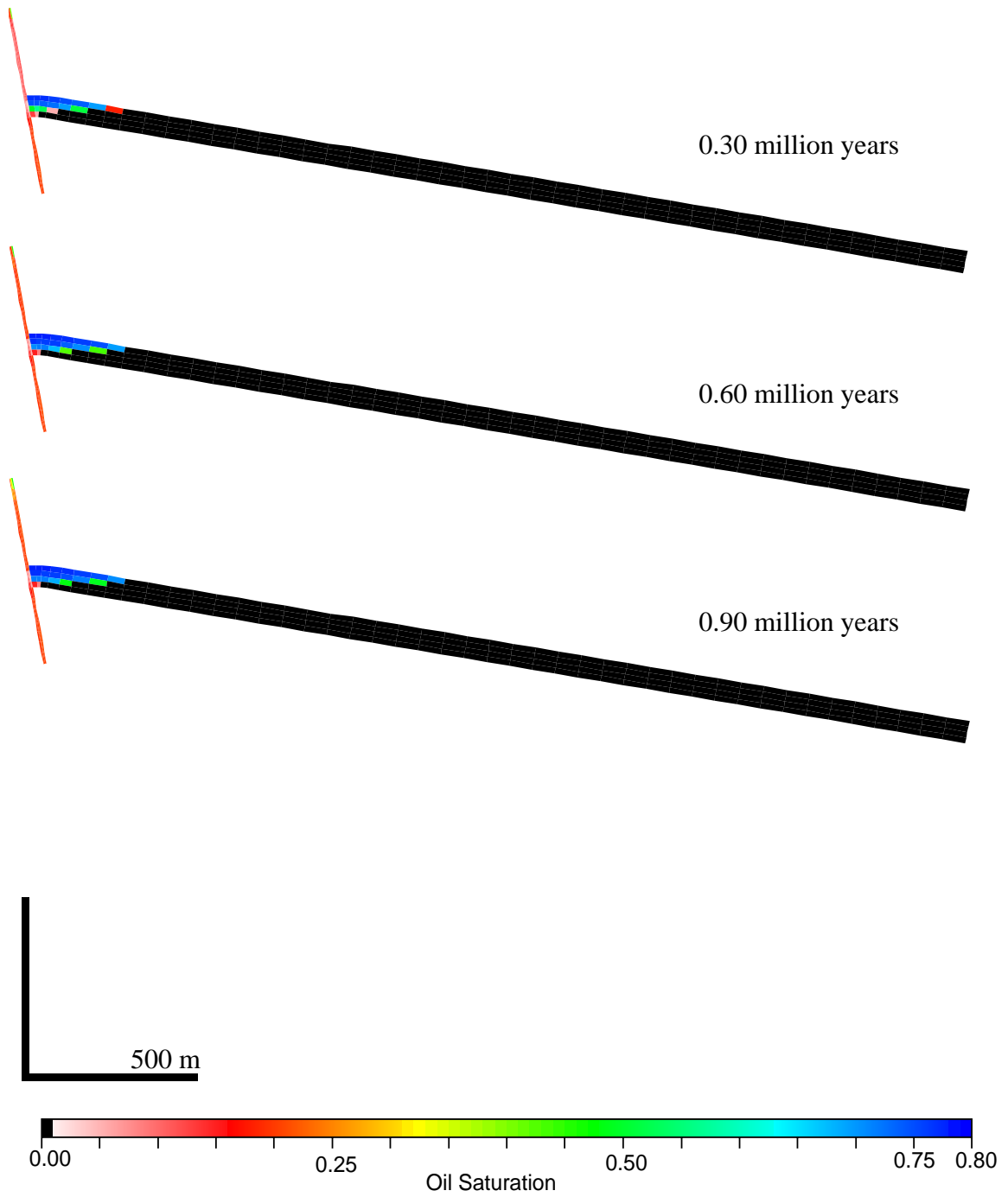
Figure 19. Saturation of oil versus location for RUN_2 at 0.30, 0.60, and 0.90 million years.

RUN_3: High Permeability Fault and Finite Reservoir

The next simulation that we present is a high permeability fault zone (0.10 millidarcies) with a finite reservoir attached. The steady-state oil saturation within the fault zone requires an analytical hydrocarbon column height of 44 meters (145 feet) in 0.5 million years.

We observe a numerical hydrocarbon column height of 42 meters (138 feet) after 1.0 million years (Figure 20). The difference in oil potential across the interface (Figure 21), the difference in water potential across the interface (Figure 22), and the relative permeability to water in the reservoir next to the interface (Figure 23) are essentially the same as in the previous example. Figure 24 is selected time slices of oil saturation versus location.
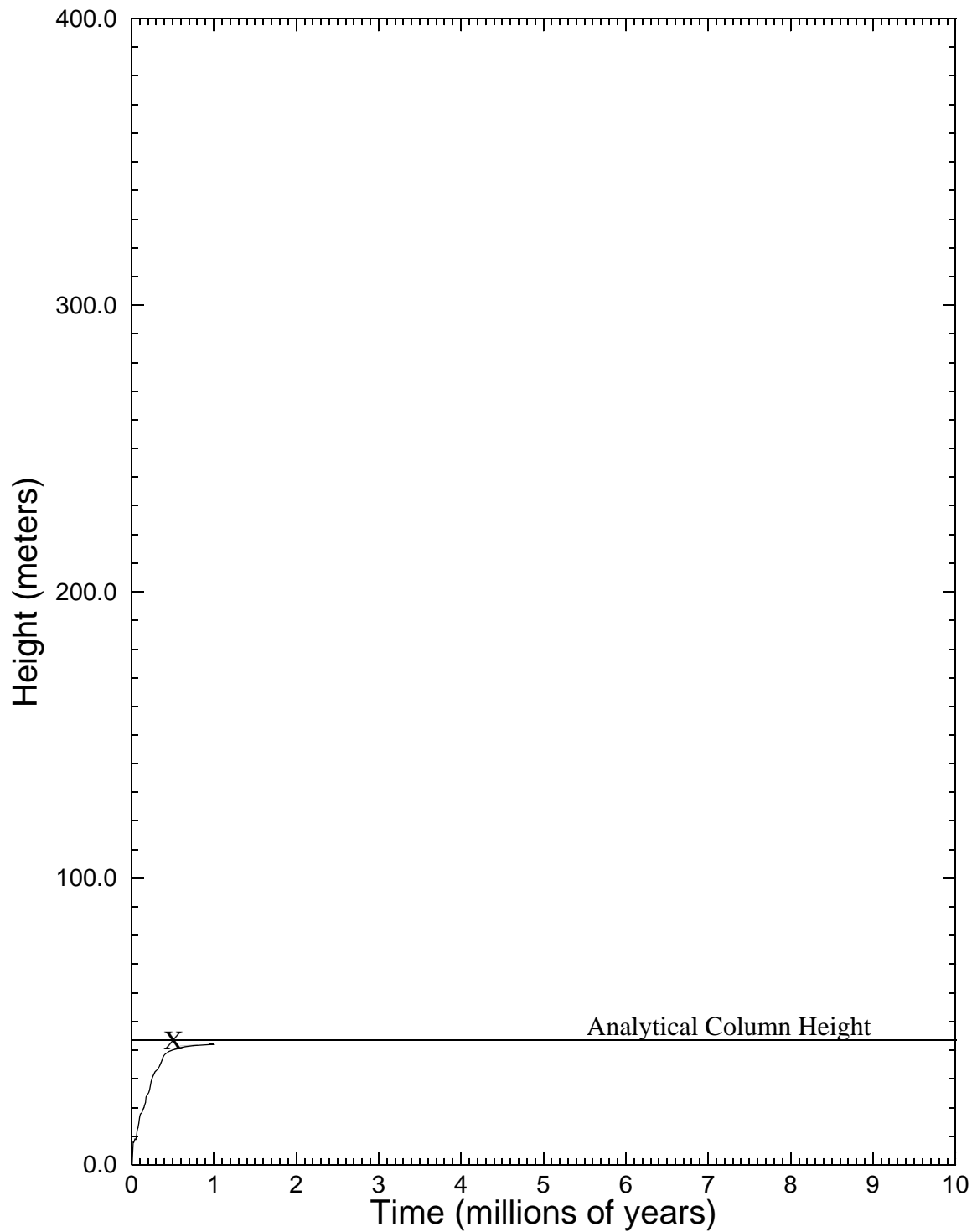
Figure 20. Hydrocarbon column height versus time for the high permeability, finite reservoir simulation (RUN_3). Steady-state height is 42 meters numerically and 44 meters analytically. The X represents the analytically calculated time required to fill the sand to a steady state hydrocarbon column of 44 meters.
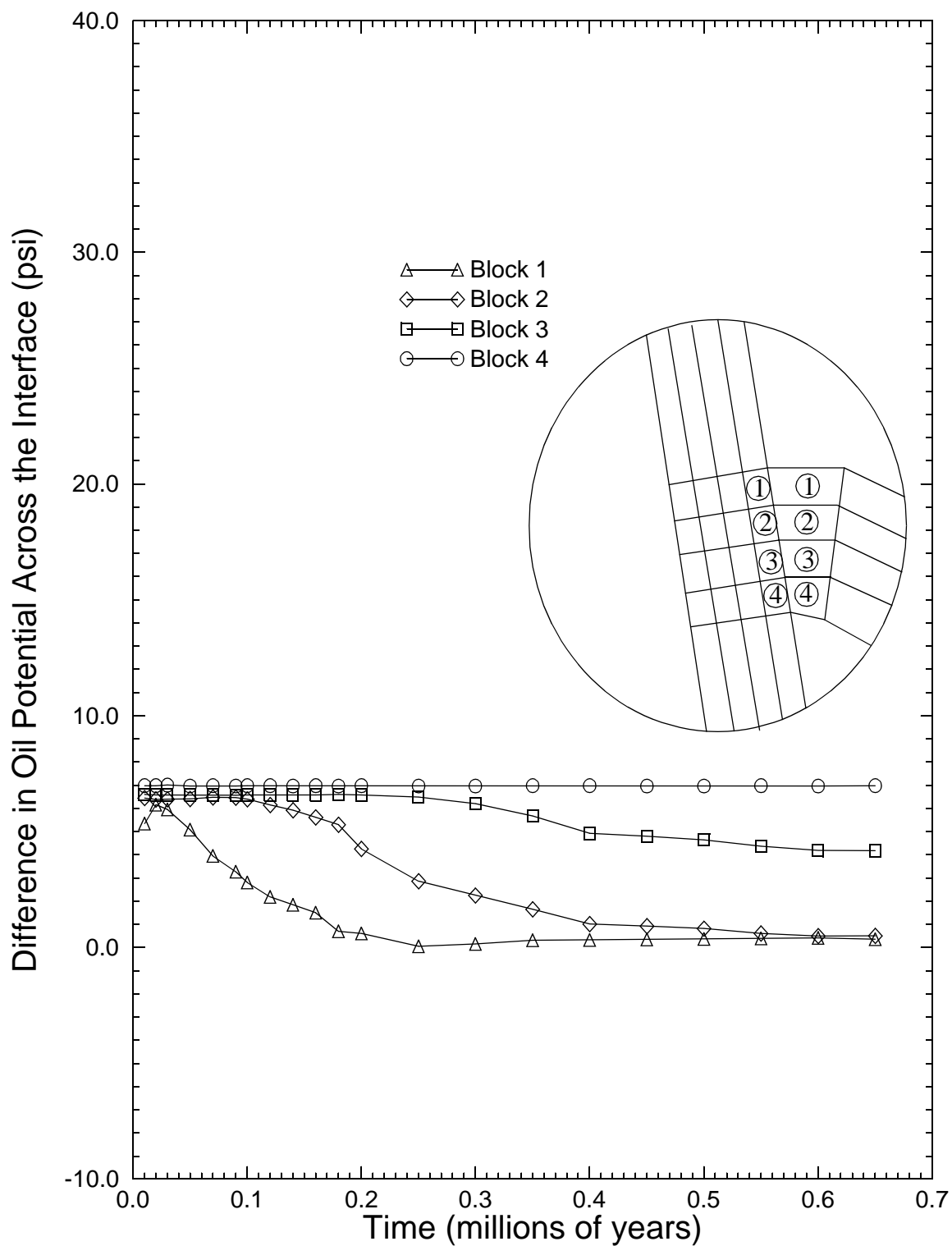
Figure 21. Difference in oil potential through time across the fault-reservoir interface for RUN_3. Values are calculated so that a positive difference in potential represents a driving force from the fault into the reservoir.
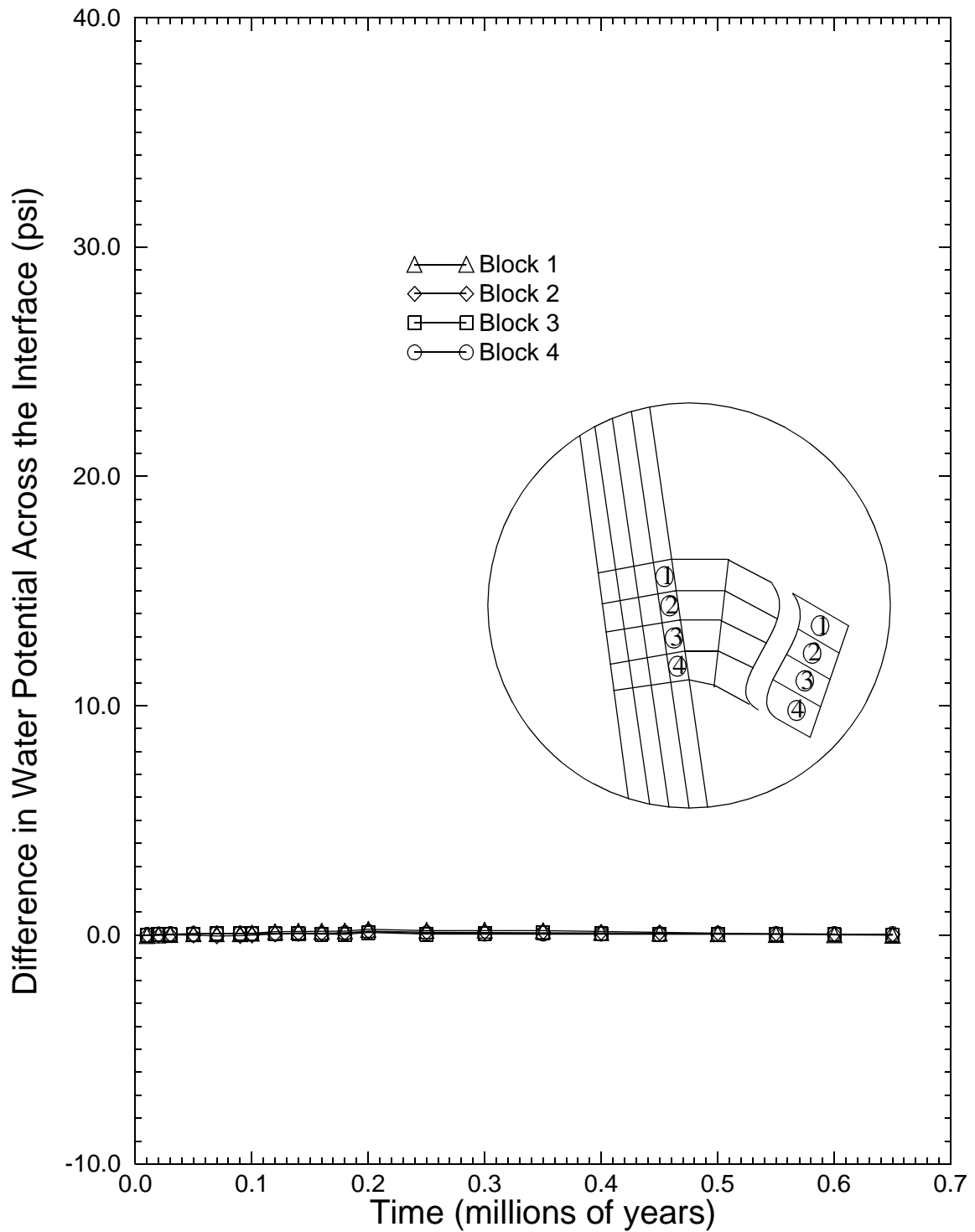
Figure 22. Difference in water potential through time from the outermost block in the sand to the first block in fault next to the interface for RUN_3. Values are calculated so that a positive difference in potential represents a driving force from the the reservoir into the fault.
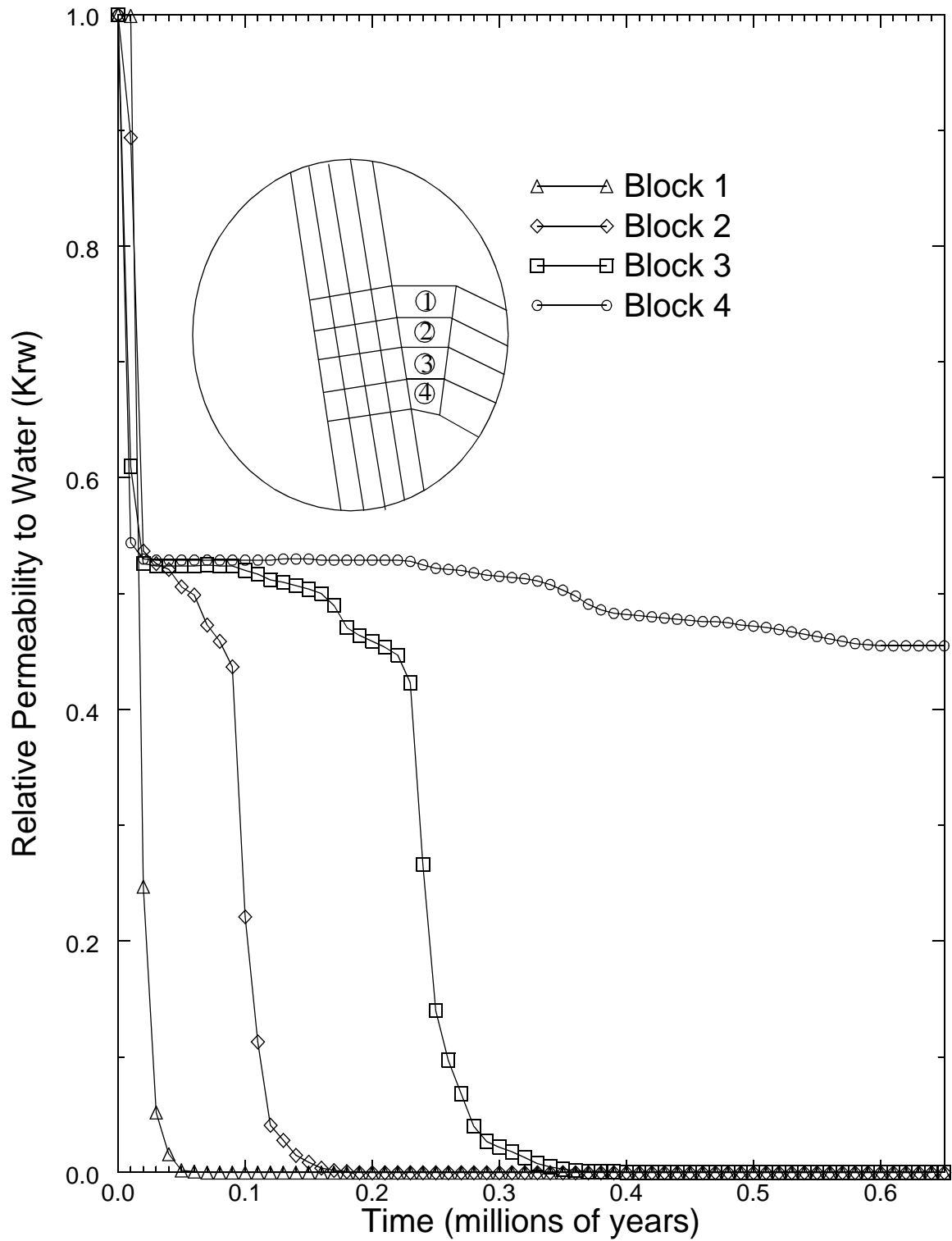
Figure 23. Relative permeability through time of the reservoir grid blocks next to the fault-reservoir interface for RUN_3.

0.30 million years

0.60 million years

0.90 million years

500 m

Oil Saturation

0.00   0.25   0.50   0.75   0.80
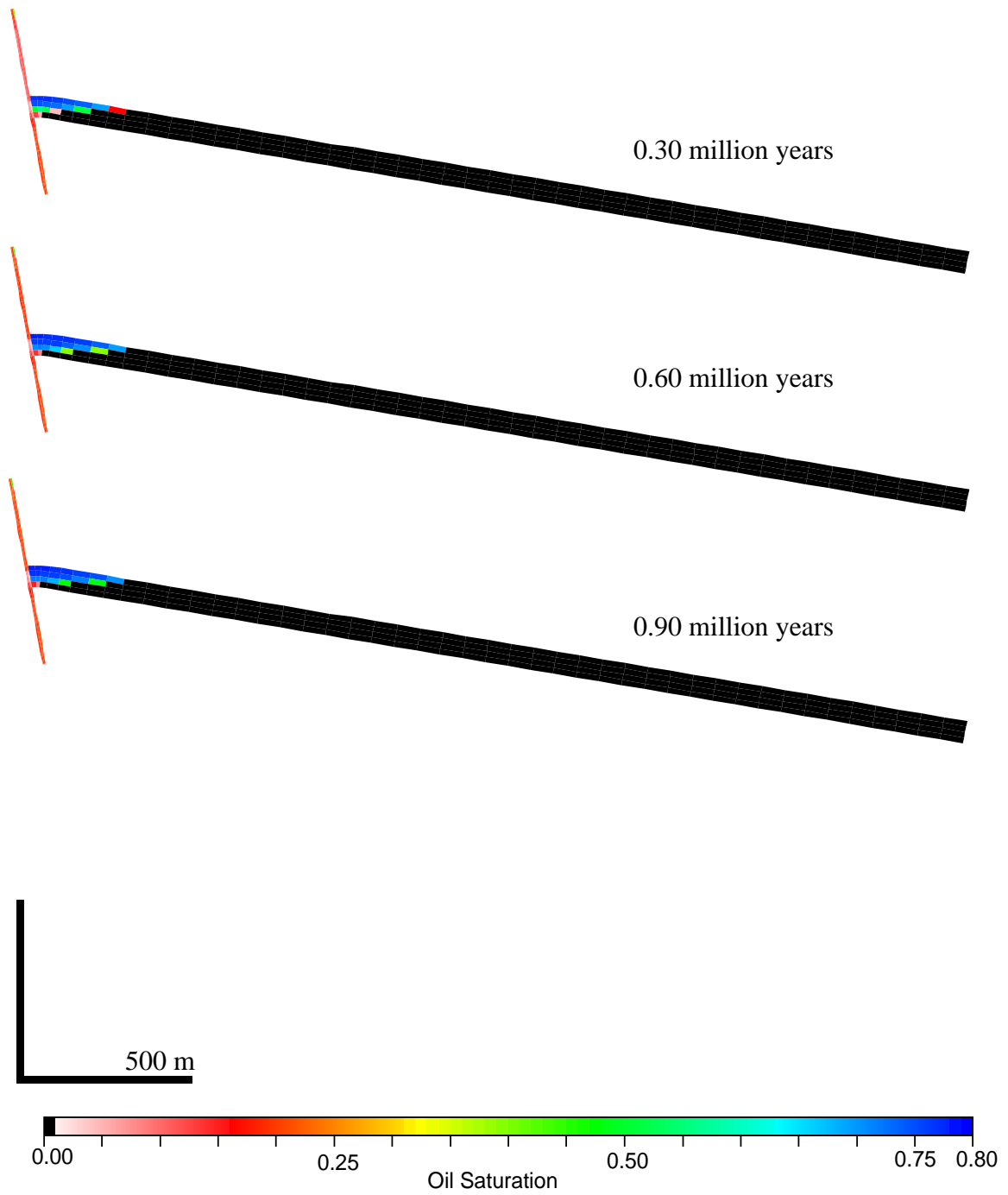
Figure 24. Saturation of oil versus location for RUN_3 at 0.30, 0.60, and 0.90 million years.

RUN_4: Low Permeability Fault and Infinite Reservoir

This simulation is identical to RUN 2 except that a low permeability (0.01 millidarcies) fault zone is simulated instead of a high permeability fault zone (0.10 millidarcies). The capillary pressure is scaled accordingly using the Leverett-J function (Equation 8 and Figure 6).

The capillary pressure and relative permeability curves from the low permeability fault example above are used as input (Figure 3 and Figure 6). The analytical methods predict a hydrocarbon column height of 347 meters (Figure 6) that should take approximately 5.8 million years to fill assuming all oil injected flows into the reservoir.

The numerical model generates a steady state hydrocarbon column height of approximately 341 meters after 10.0 million years of simulation time (Figure 25). We note that initially, infilling of the reservoir is rapid and apparently linear with respect to time (Figure 25). Almost all the oil injected enters the reservoir at early times and very little flows up the fault past the reservoir. This is apparent in Figure 29, where we see very low oil saturations in the fault zone, at early times, above the fault-reservoir interface. When the steady-state column height is approached filling of the reservoir slows. Figure 26 illustrates that as the reservoir fills, the difference in oil potential across the fault-reservoir interface (i.e. the driving potential of oil from the fault into the reservoir) decreases until about 3.5 million years, at which point the difference in oil potential across the interface levels off. This corresponds to the point in Figure 25 where there is a distinct departure from the apparent linear trend of hydrocarbon column height versus time towards a lognormal trend. Water potential differences between the fault blocks adjacent to the reservoir and blocks in the farthest reaches of the reservoir are small relative to the differences in oil
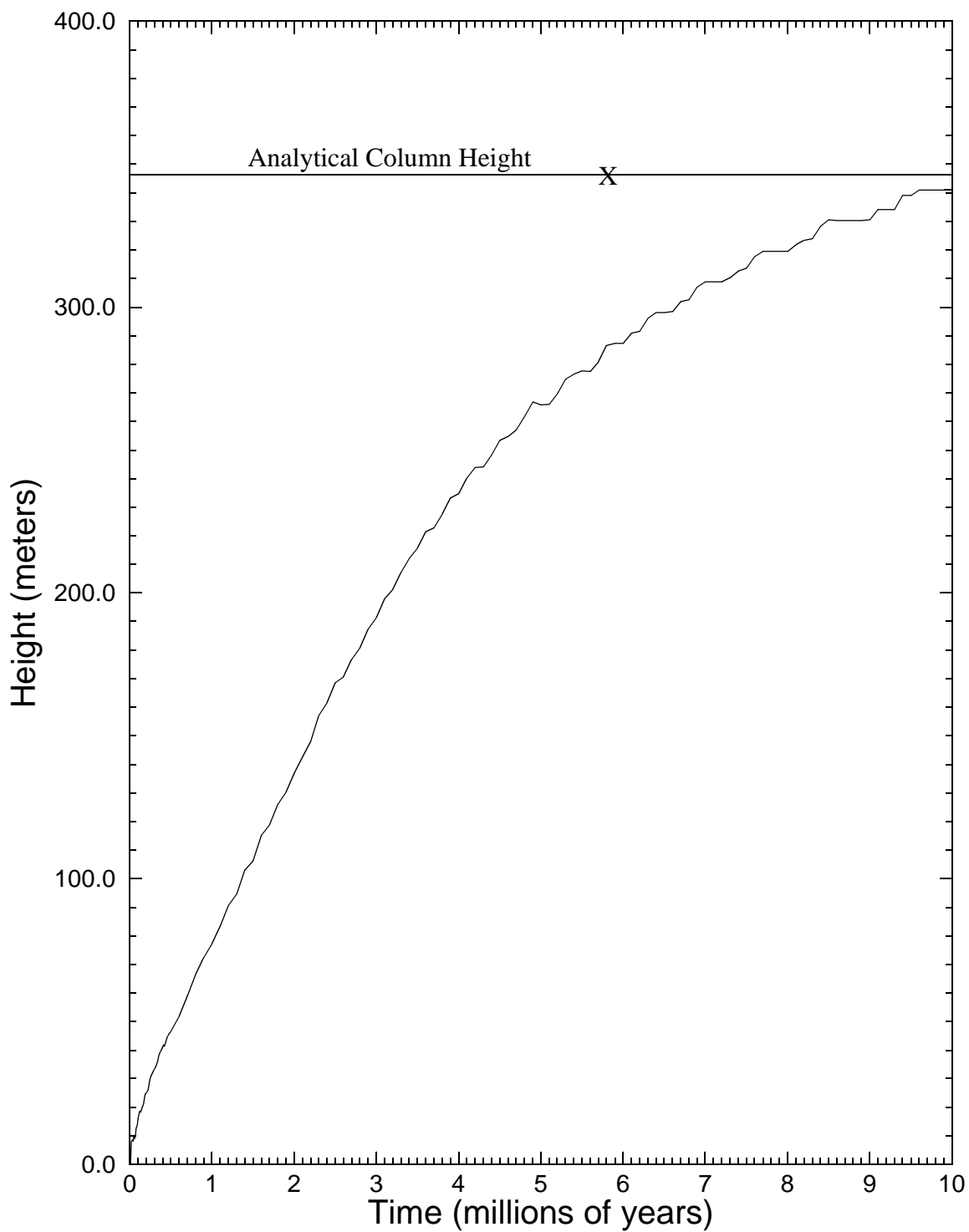
Figure 25.   Hydrocarbon column height versus time for the low permeability, infinite reservoir simulation (RUN_4). Steady-state height is 341 meters numerically and 347 meters analytically. The X represents the analytically calculated time required to fill the sand to a steady state hydrocarbon column of 347 meters.
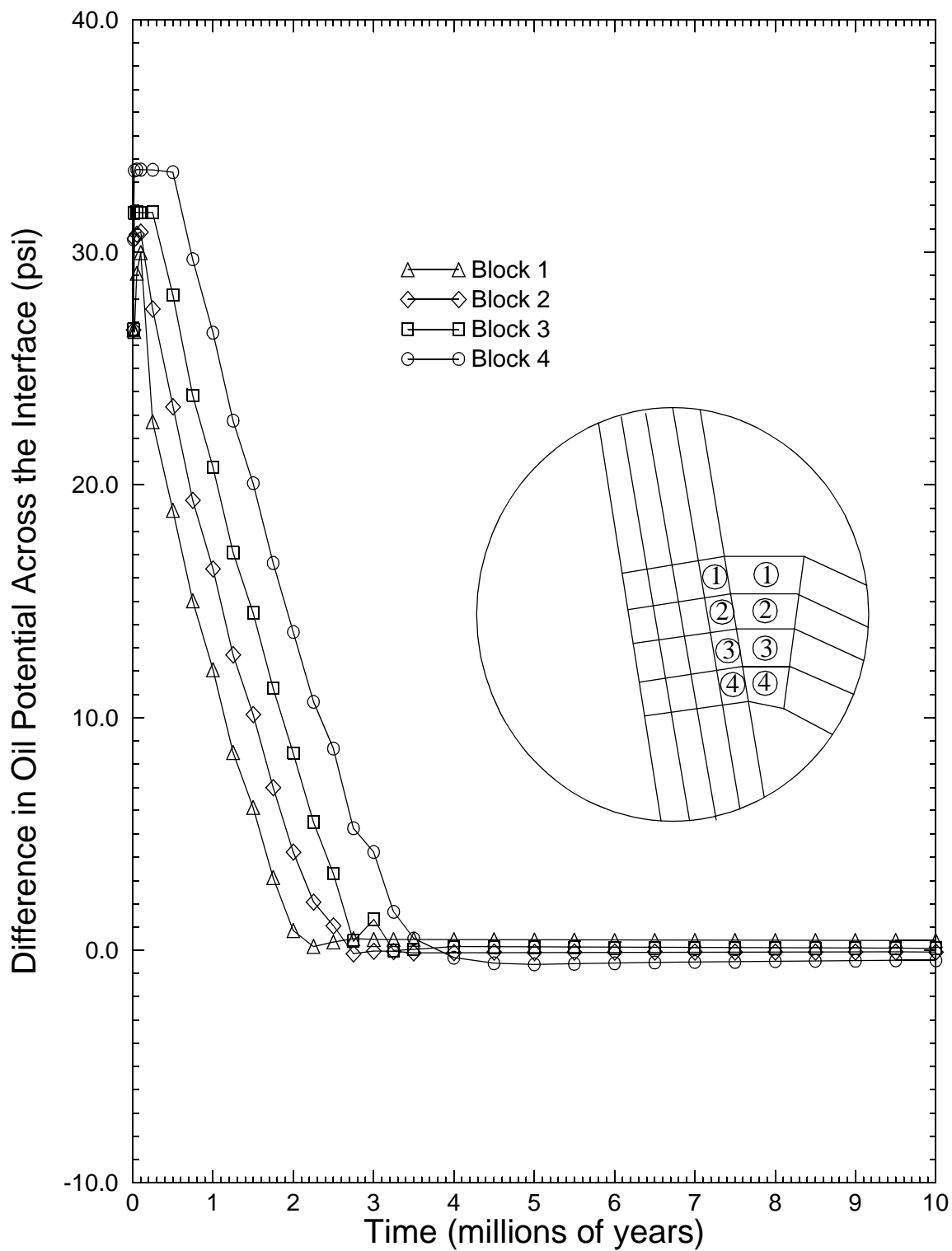
Figure 26. Difference in oil potential through time across the fault-reservoir interface for RUN_4. Values are calculated so that a positive difference in potential represents a driving force from the fault into the reservoir.

potential illustrating that water has little driving potential from the reservoir to the fault (Figure 27). This is due to the constant pressure boundary at the periphery of the sand (Figure 7a).

Due to the increase in oil saturation, a reduction in water relative permeability is observed through time in the reservoir blocks at the fault-reservoir interface (Figure 28). After 0.55 million years the relative permeability to water is essentially zero in the reservoir along the interface. Until about 0.55 million years, water may escape from the reservoir to the fault zone, after that point in time, however, the water in the reservoir may not escape and must move down into the infinite reservoir ahead of the entering oil.

This significant reduction of water relative permeability is due primarily to the shape of the capillary pressure curve and the irreducible water saturation (Figure 6 and Figure 3). The shape of the capillary pressure curve for the reservoir dictates the saturation of oil at the top of the reservoir (Figure 6). The irreducible water saturation is specified via CoreyÕs Approximation (Figure 3). For our example, the shape of the reservoirÕs capillary pressure curve requires that the saturation at the top of reservoir approach irreducible water saturation. This causes the relative permeability to drop to zero.

Figures 29 through 31 are selected time slices of oil saturation versus location. Figure 29 shows that at 0.5 million years the oil-water contact in the reservoir approaches the thickness of the reservoir.
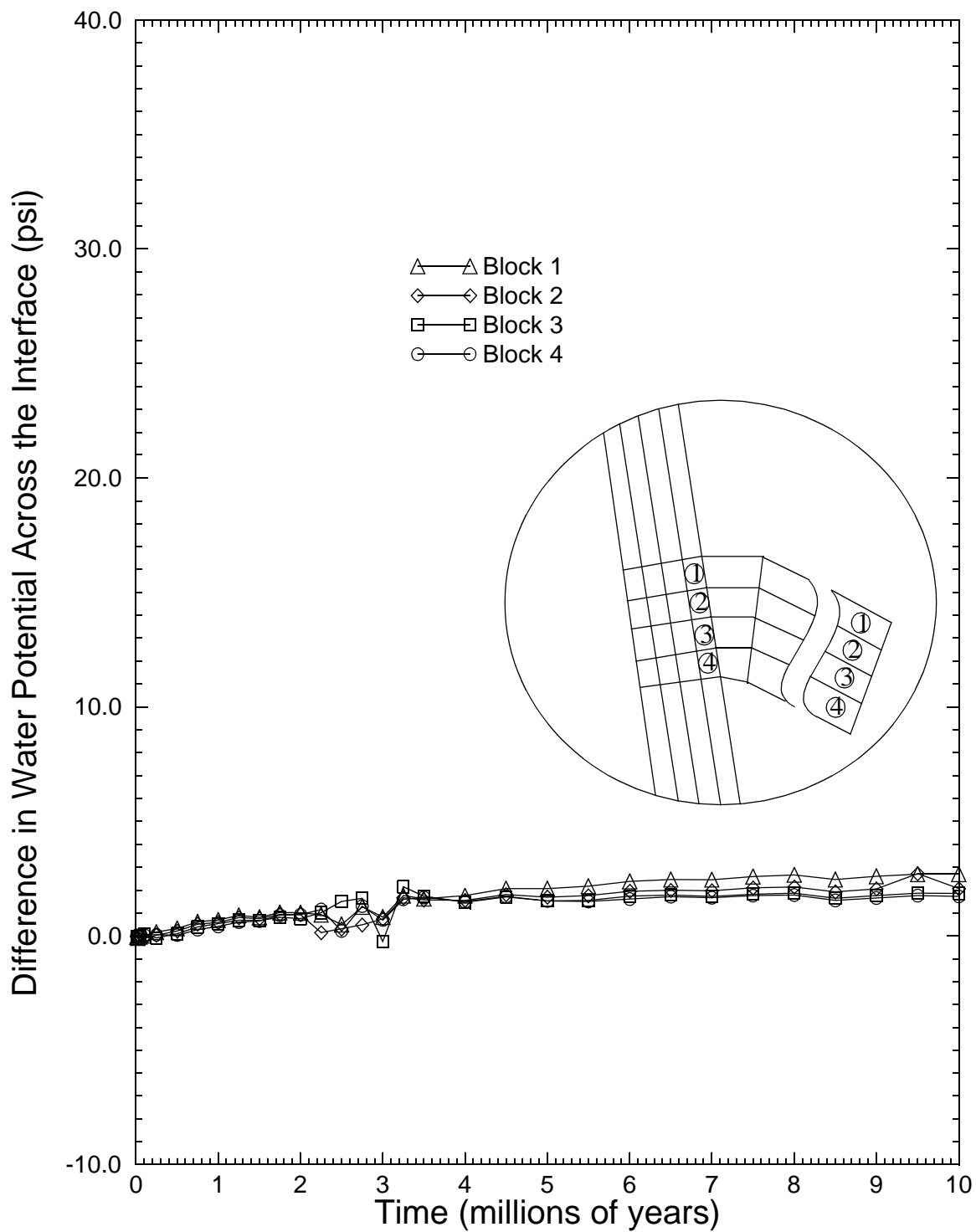
Figure 27. Difference in water potential through time from the outermost block in the sand to the first block in fault next to the interface for RUN_4. Values are calculated so that a positive difference in potential represents a driving force from the the reservoir into the fault.
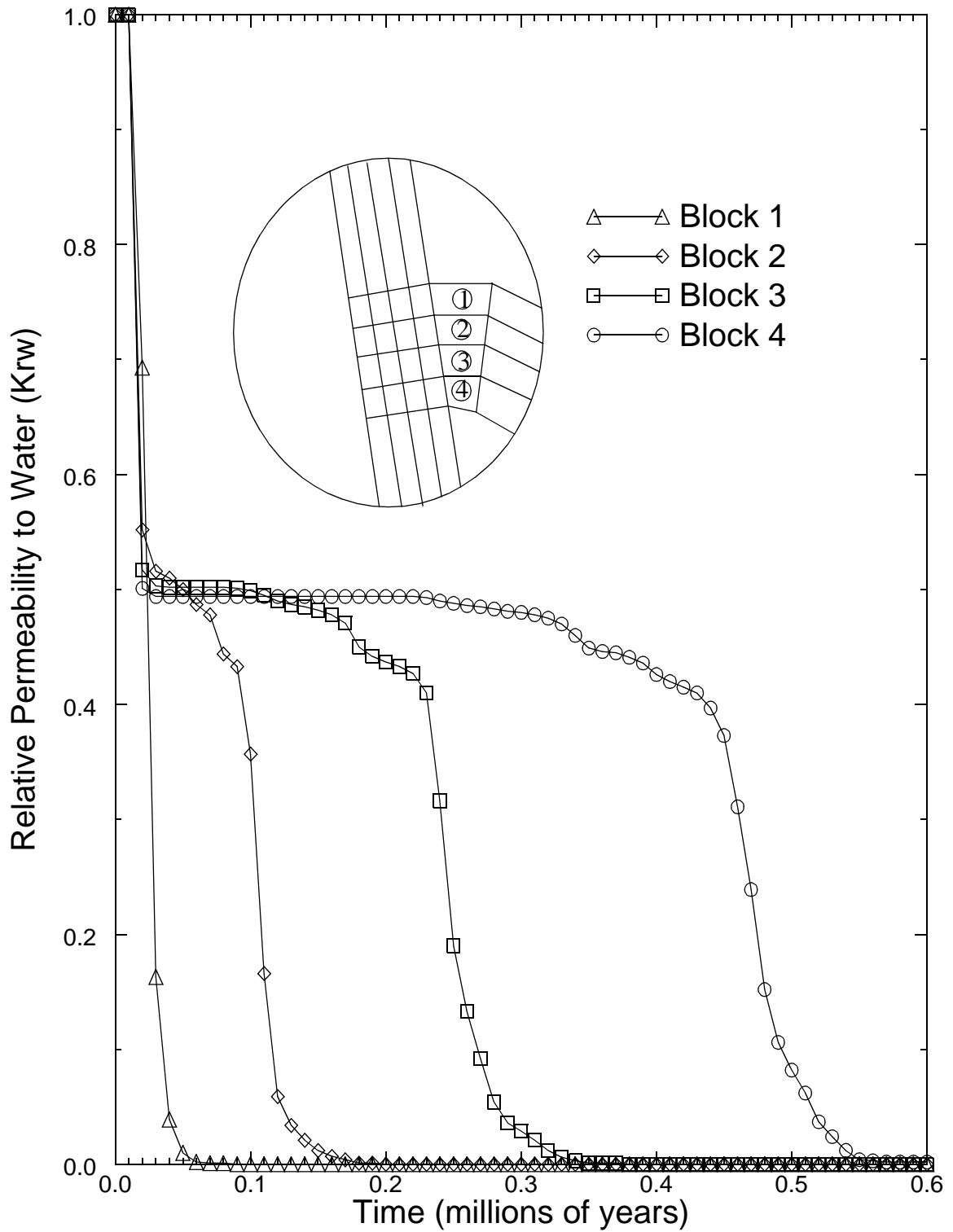
Figure 28. Relative permeability through time of the reservoir grid blocks next to the
fault-reservoir interface for RUN_4.

0.5 million years

1.0 million years

2.0 million years

3.0 million years

500 m

0.00   0.25   0.50   0.75   0.80
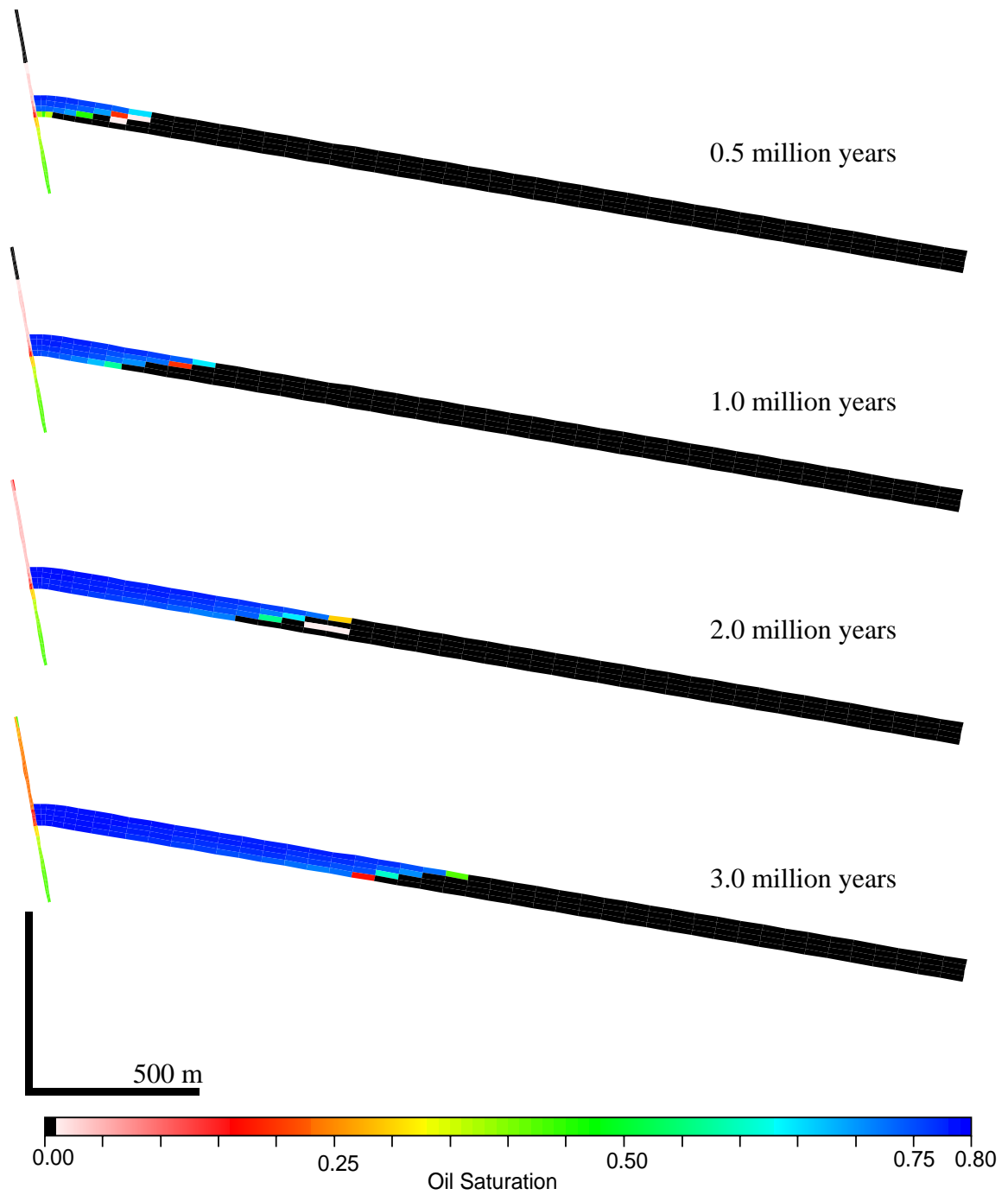
Oil Saturation

Figure 29. Saturation of oil versus location for RUN_4 at 0.5, 1.0, 2.0, and 3.0 million years.
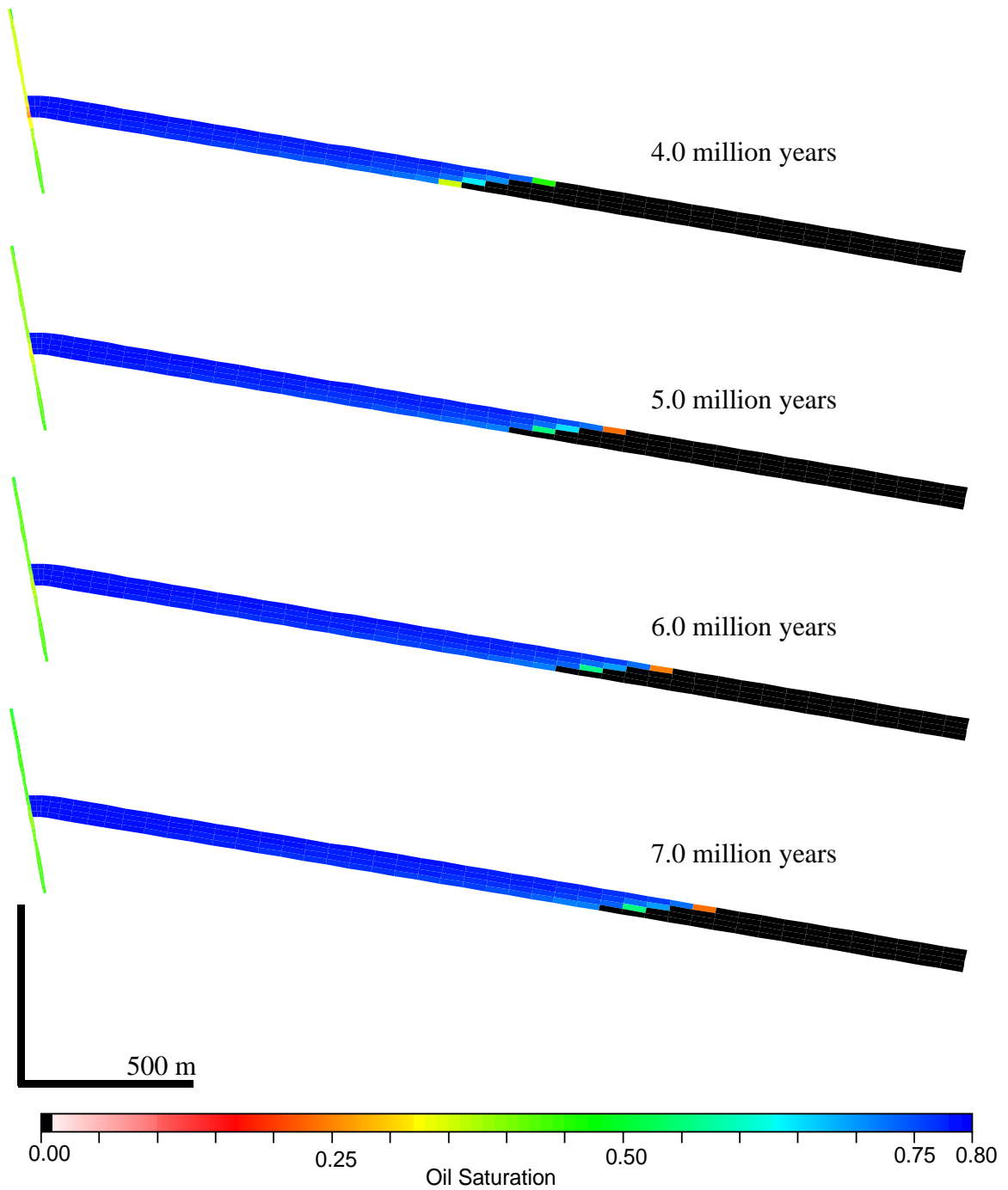
Figure 30. Saturation of oil versus location for RUN_4 at 4.0, 5.0, 6.0, and 7.0 million years.

8.0 million years

9.0 million years

10.0 million years

500 m

Oil Saturation
0.00　　　　0.25　　　　0.50　　　0.75　0.80
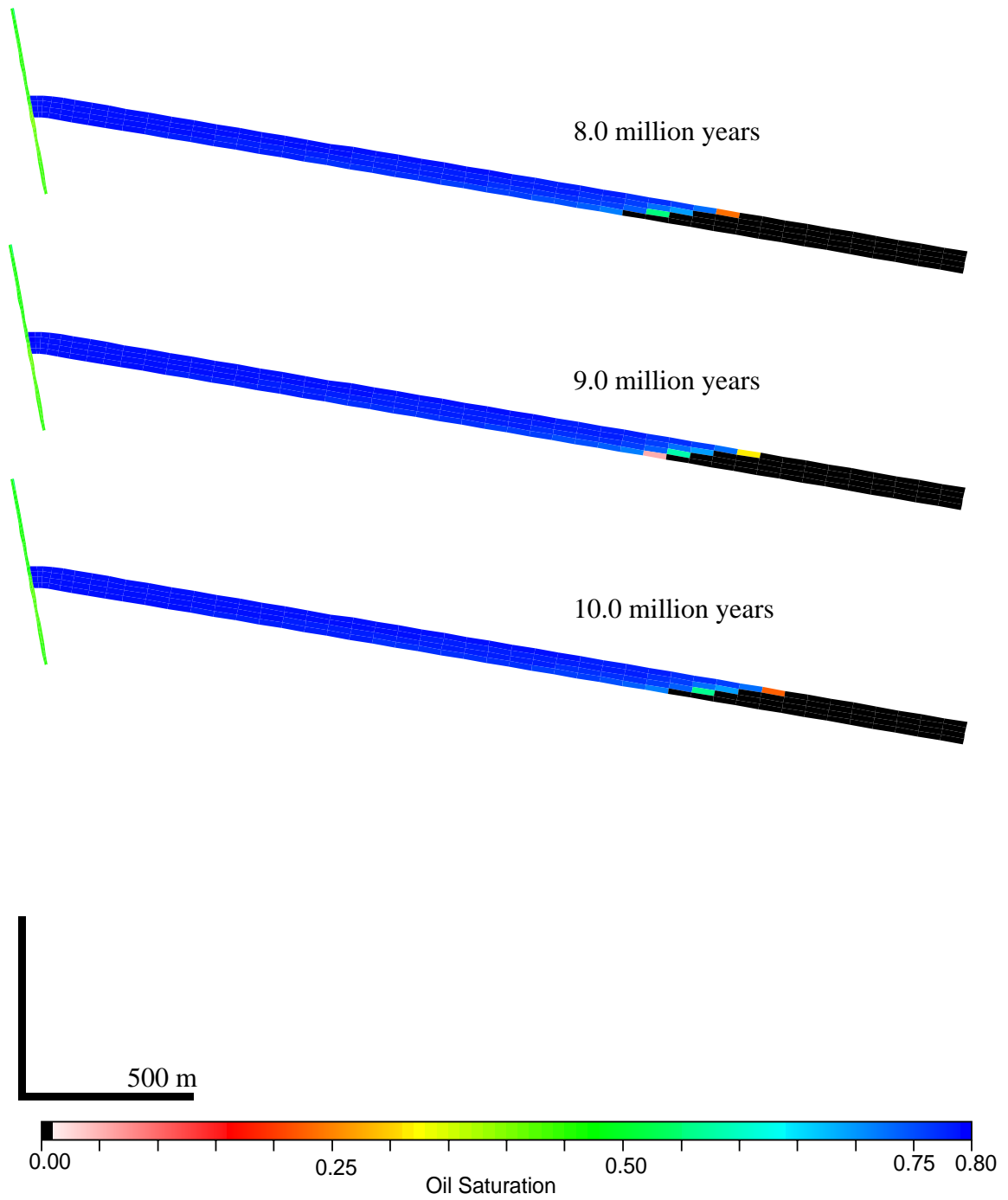
Figure 31. Saturation of oil versus location for RUN_4 at 8.0, 9.0, and 10.0 million years.

RUN_5: Low Permeability Fault and Finite Reservoir

The next simulation we investigate is identical to the previous simulation with the exception that instead of an infinite reservoir a finite reservoir is attached to the fault zone (Figure 8b). This is accomplished by imposing a no-flow boundary at the down dip end of the reservoir (Figure 7b). From the analytical methods described in this paper we predict a hydrocarbon column height of 347 meters and a fill time of approximately 5.8 million years, the same as the previous simulation.

The numerical model generates a steady state hydrocarbon column height of 58 meters after 1.1 million years (Figure 32) and a significant departure from the previous simulationÕs results (Figure 25) after 0.5 million years. Initially, the reservoir fills quickly with hydrocarbons from the fault zone. After 0.5 million years, however, we observe a distinct drop in the rate of hydrocarbons filling the reservoir (Figure 32). The difference in oil potential from the fault zone into the reservoir drops to low values after 0.5 million years (Figure 33). A concurrent rise in the difference in water potential from the reservoir into the fault is illustrated in Figure 34.

The relative permeability to water in the reservoir at the interface exhibits the same trend for this case as the previous simulation (Figure 28 and Figure 35). That is, the relative permeability of water drops to nearly zero in all the grid blocks of the reservoir next to the interface. After 0.5 million years, oil flow into the reservoir is essentially stopped because the reservoir pressure has increased due to the compression of trapped or ÒPerchedÓ water. In the previous example this pressure was released across the constant pressure boundary. It is this drop in relative permeability that is causing the rise and drop
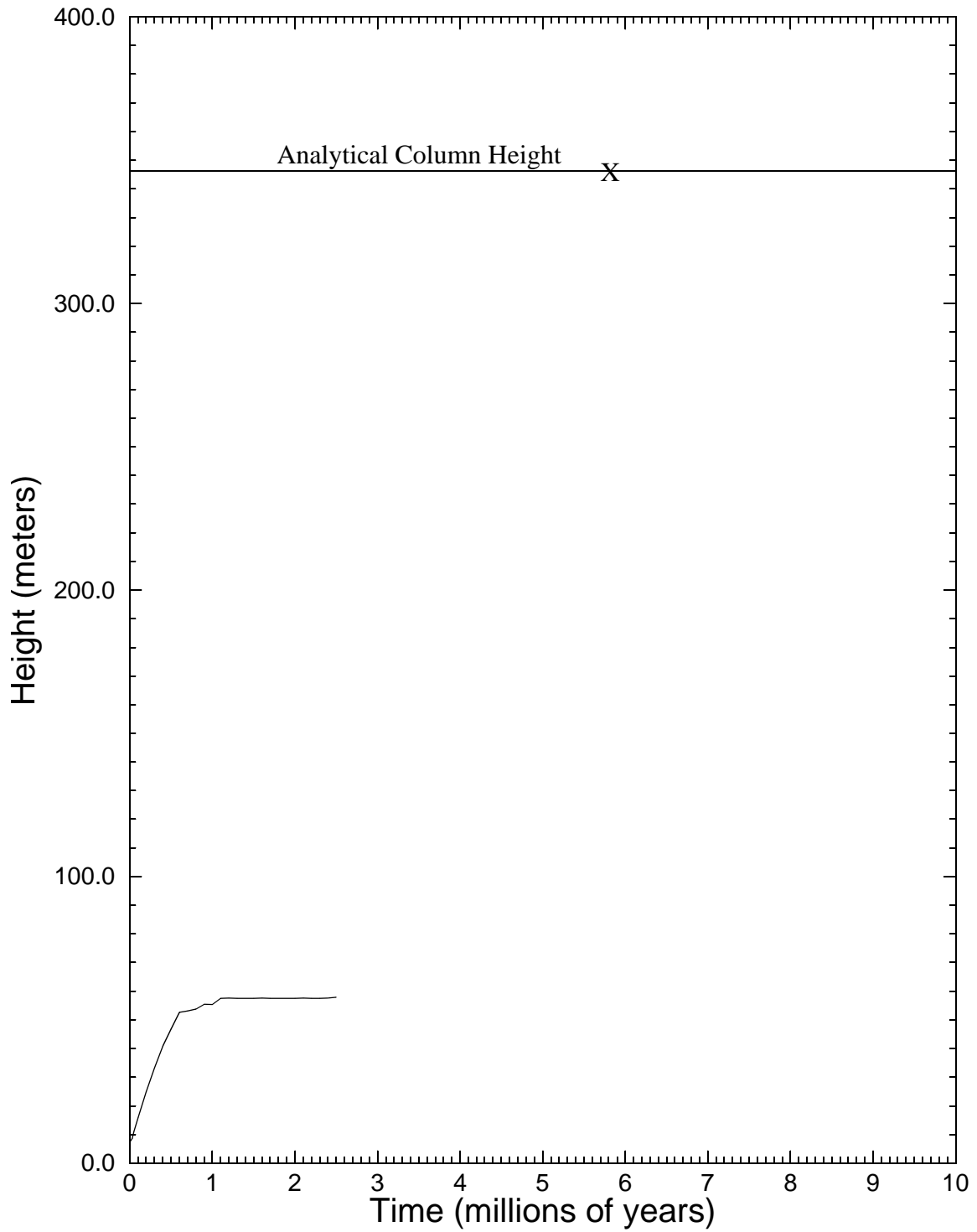
Figure 32. Hydrocarbon column height versus time for the low permeability, finite reservoir simulation (RUN_5). Steady-state height is 58 meters numerically and 347 meters analytically. The X represents the analytically calculated time required to fill the sand to a steady state hydrocarbon column of 347 meters.
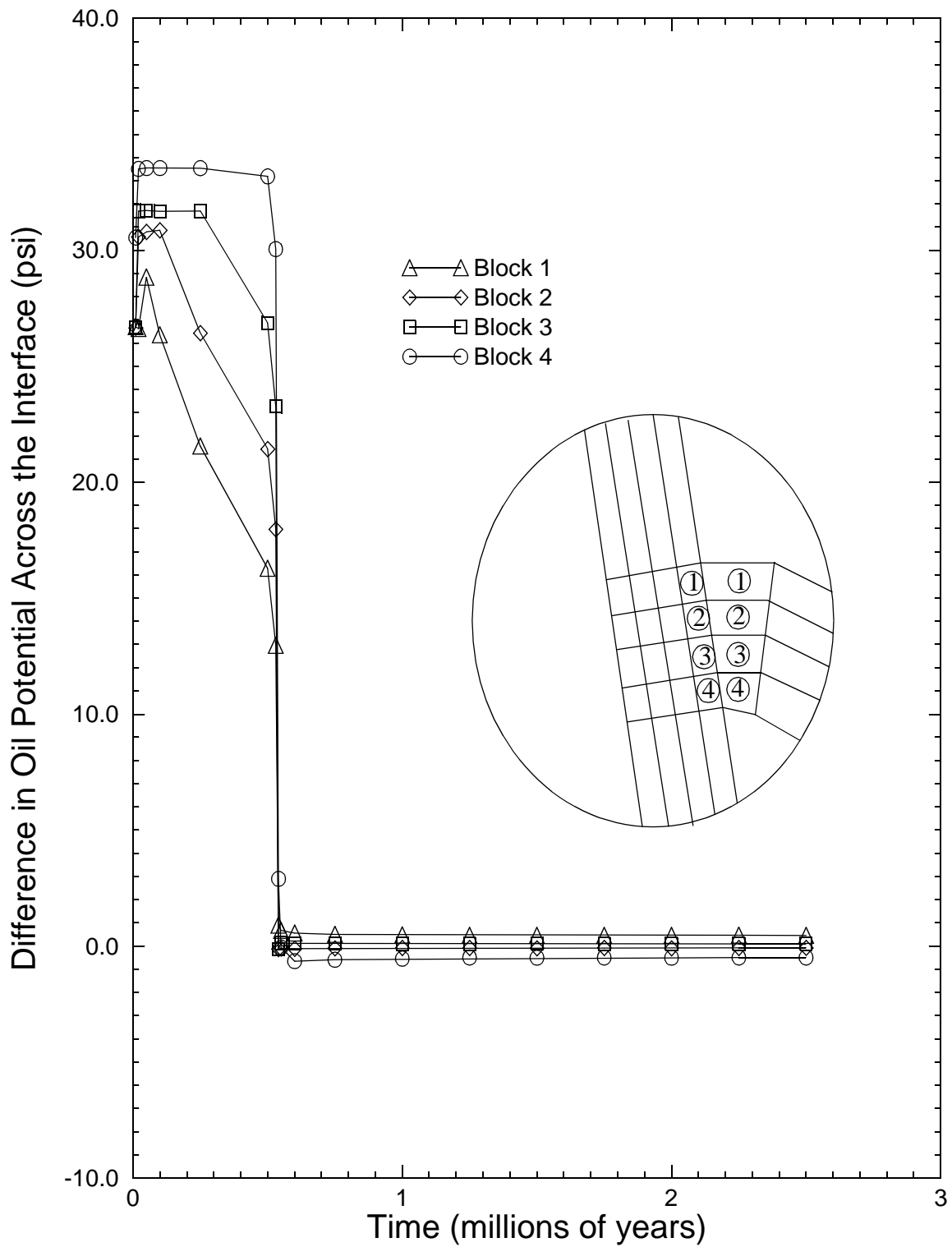
Figure 33. Difference in oil potential through time across the fault-reservoir interface for RUN_5. Values are calculated so that a positive difference in potential represents a driving force from the fault into the reservoir.
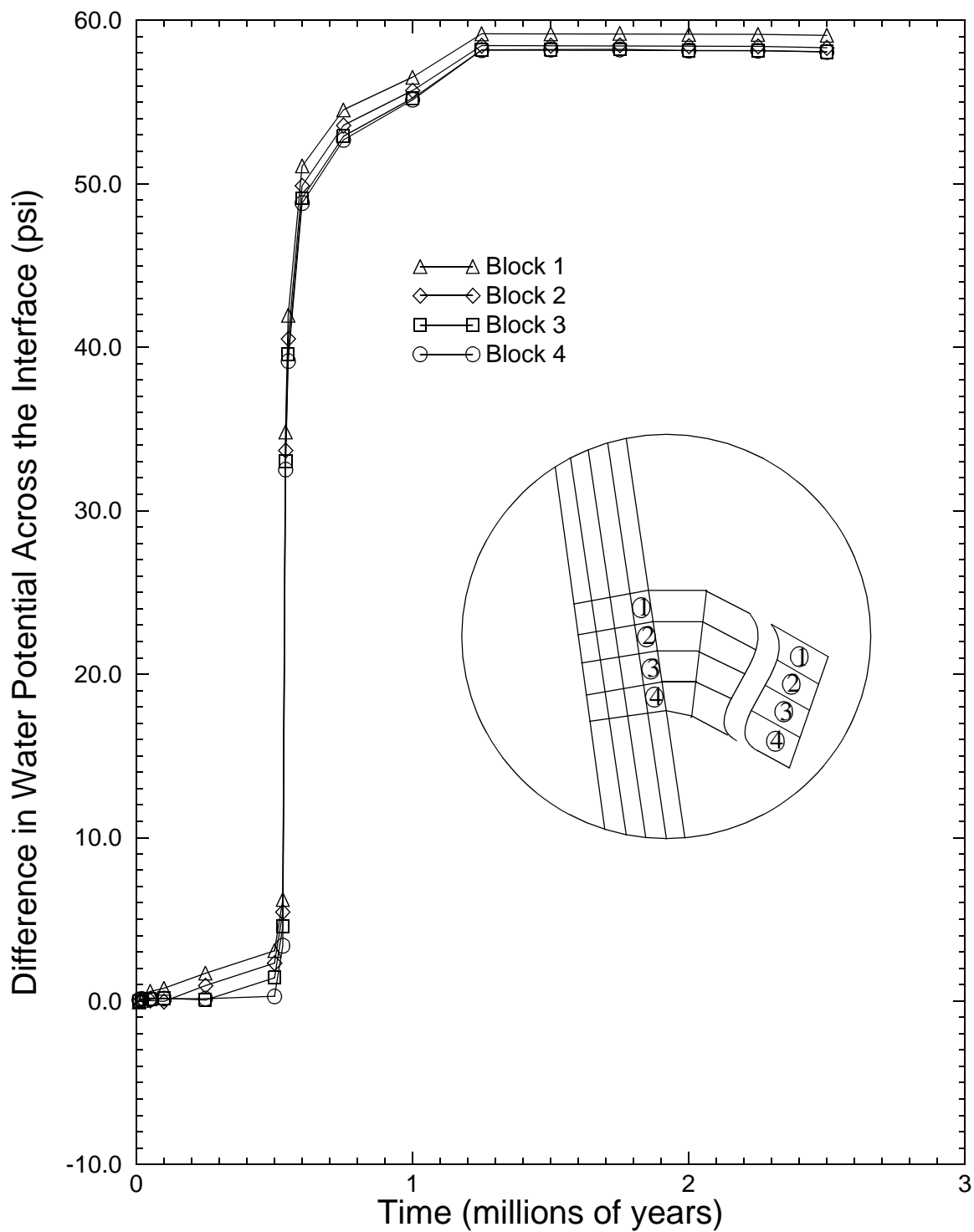
Figure 34. Difference in water potential through time from the outermost block in the sand to the first block in fault next to the interface for RUN_5. Values are calculated so that a positive difference in potential represents a driving force from the the reservoir into the fault.
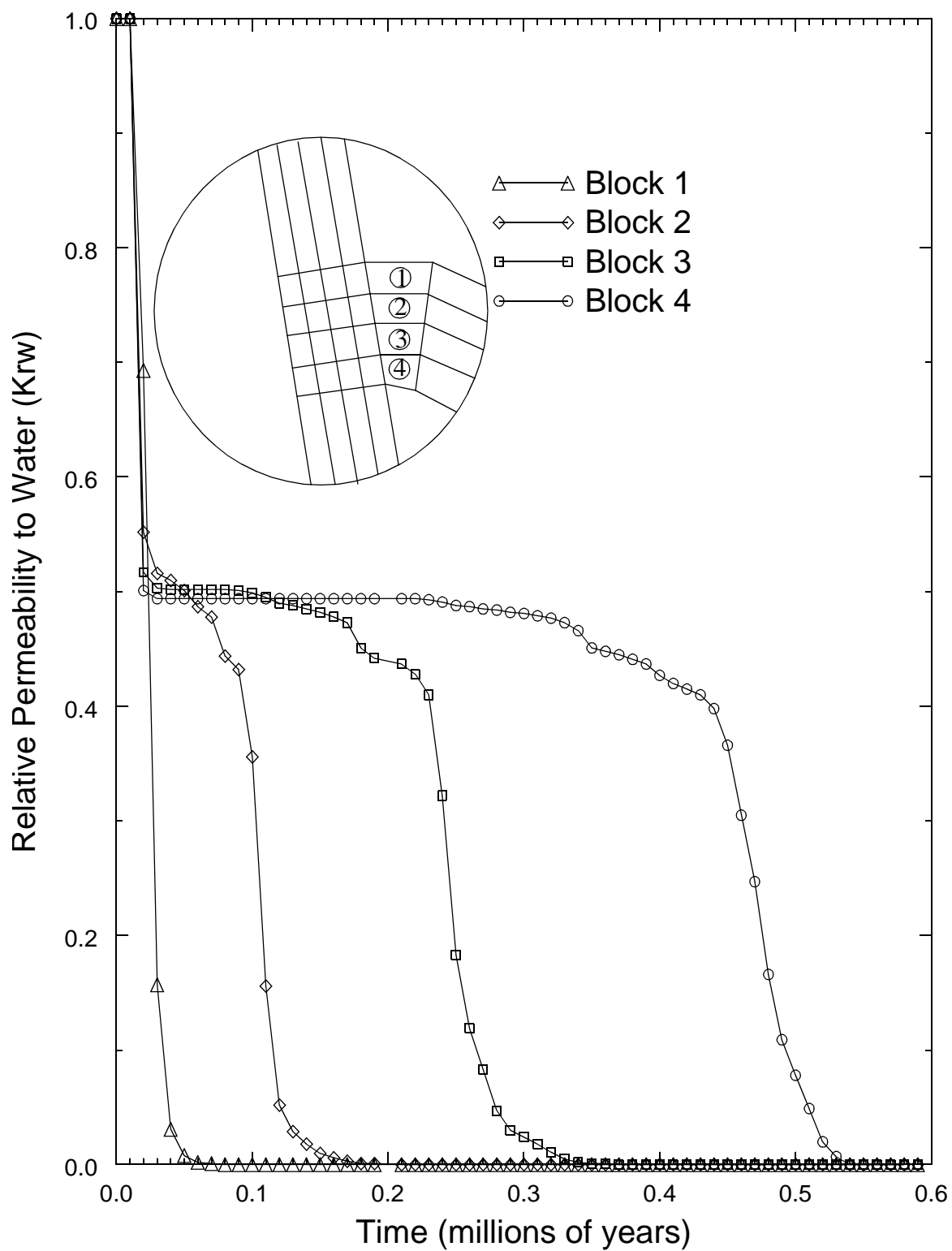
Figure 35. Relative permeability through time of the reservoir grid blocks next to the fault-reservoir interface for RUN_5.

in water and oil potential differences, respectively.

Figure 36 is selected time slices of oil saturation versus location. Figure 36 shows no apparent change in the oil water contact from 1.50 to 2.25 million yearsm, illustrating that the system is nearly at steady-state.

0.25 million years

0.75 million years

1.50 million years

2.25 million years

500 m

0.00　　　　　　0.25　　　　　　0.50　　　　0.75　0.80
Oil Saturation
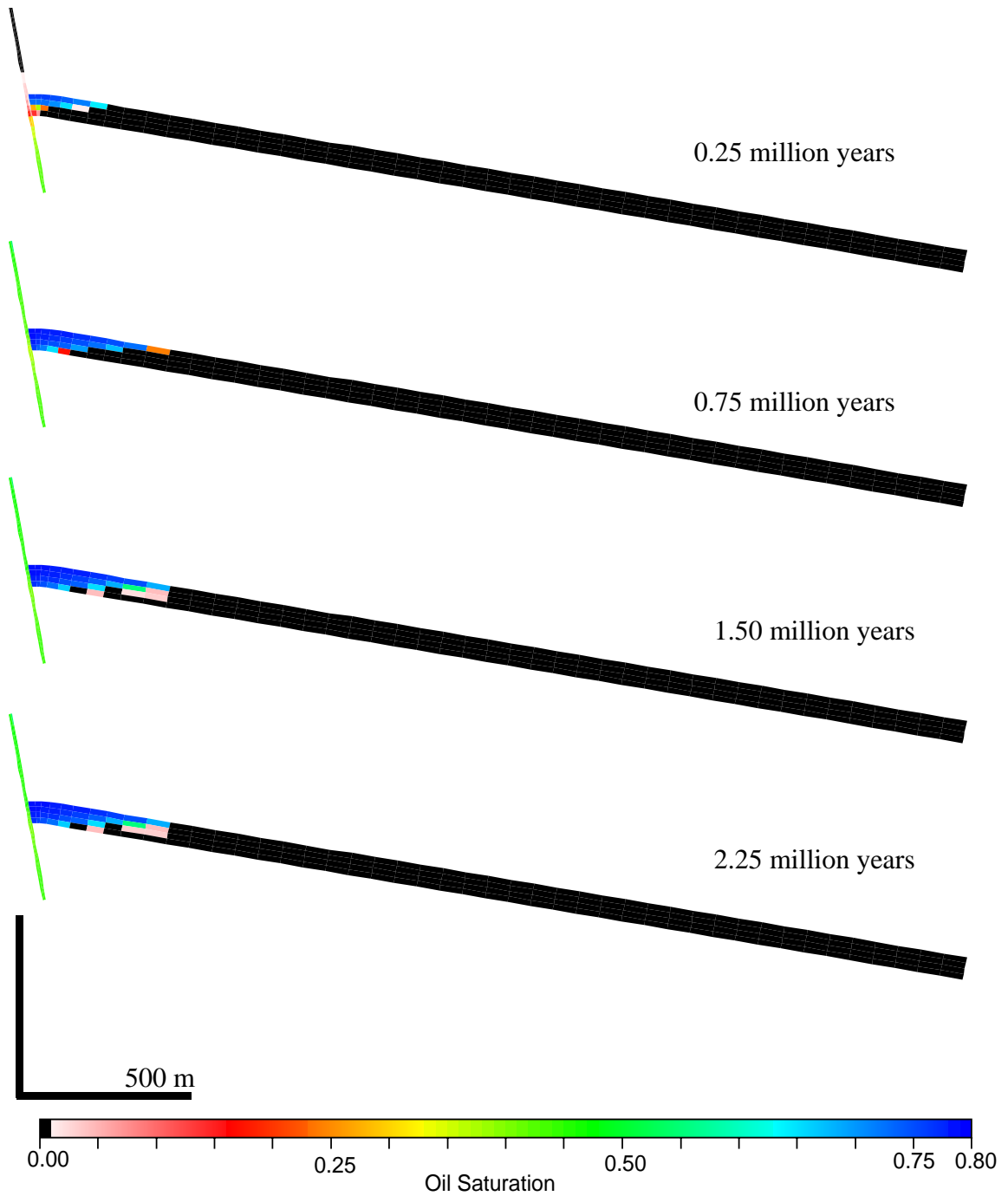
Figure 36. Saturation of oil versus location for RUN_5 at 0.25, 0.75, 1.50, and 2.25 million years.
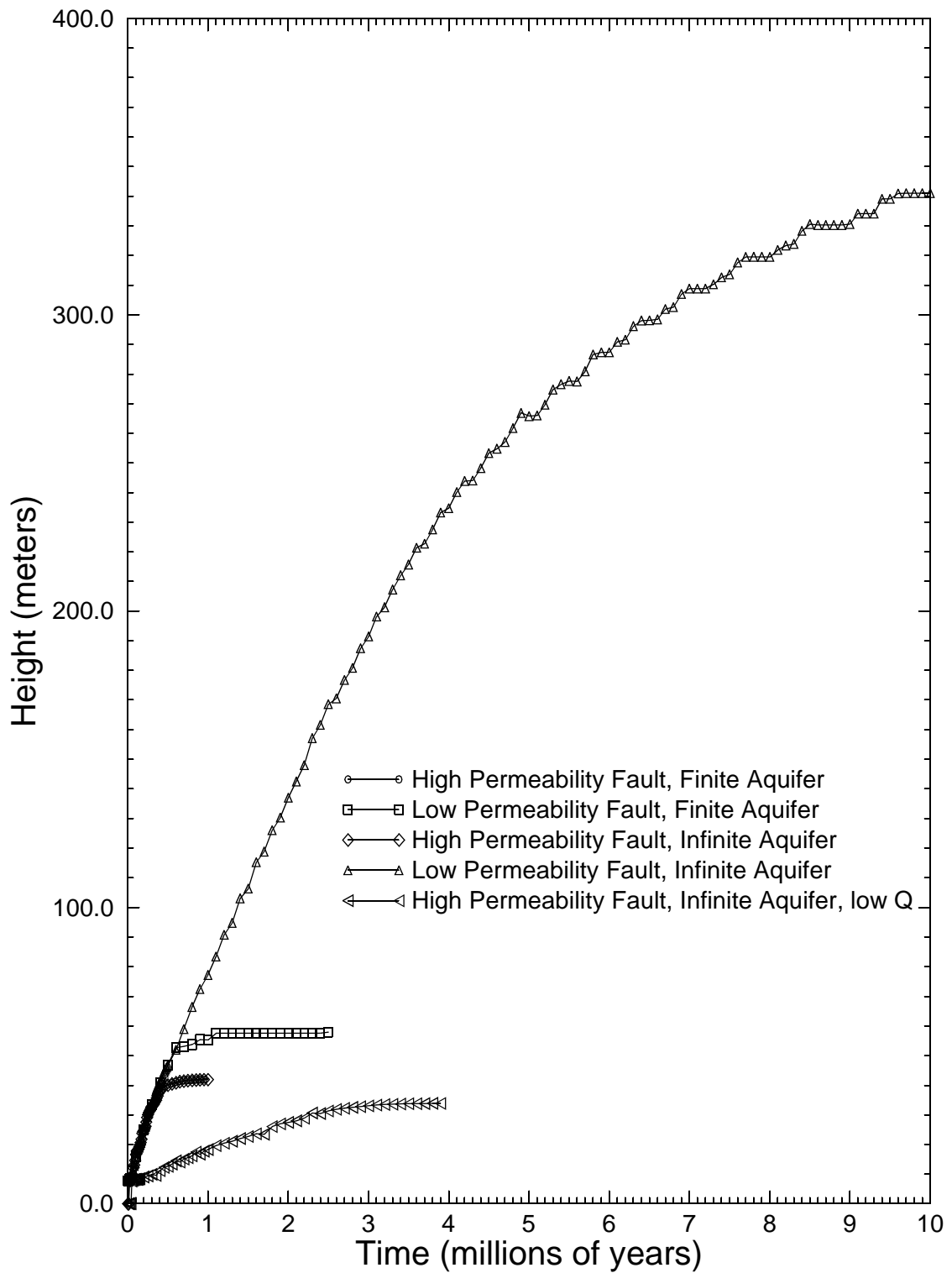
Figure 37. Summary of oil column height versus time for RUN_1, RUN_2, RUN_3, RUN_4, and RUN_5.

RUN_6: Complex Fault and Multiple Reservoirs

The last numerical simulation is a relatively complex geological model. The fault zone is divided into two regions. The lower section of the fault zone has a permeability of 0.01 millidarcies and the upper section of the fault zone has a permeability of 0.10 millidarcies (Figure 38). Geologically, this variation of permeability within the fault zone can be attributed to shale smear. A large shale sequence, more susceptable to ductile deformation and smearing, located below the first two reservoirs could cause more shale smear (lower permeability) in the deeper portion of the fault zone as opposed to the shallow portion of the fault zone.

Connected to this fault are a total of four reservoirs. Two reservoirs, one finite and one infinite, are connected to both the upper and lower sections of the fault zone. The reservoirs on the downthrown side of the fault zone dip 20 degrees and the reservoirs on the upthrown side of the fault zone dip 10 degrees. Using the analytical approach developed in this paper, we expect oil column heights of 44 meters in both the reservoirs attached to the high permeability fault zone and oil column heights of 347 meters in both the reservoirs attached to the low permeability fault zone. Note that in this model we are predicting a large range of oil columns to demonstrate the geological complexity of this system. We propose that this complex model is a more attainable analogy to real systems that we observe in the field.

Our numerical model generates oil column heights of 47 meters for the finite reservoir attached to the high permeability fault section, 53 meters for the infinite reservoir attached to the high permeability fault section, 70 meters for the finite reservoir attached to the low permeability fault section, and 293 meters for the infinite reservoir attached to the low per-

meability fault section (Figure 39).

High Permeability Fault

Low Permeability Fault

Figure 38. Conceptual model of the complex fault and multiple reservoirs of RUN_6.
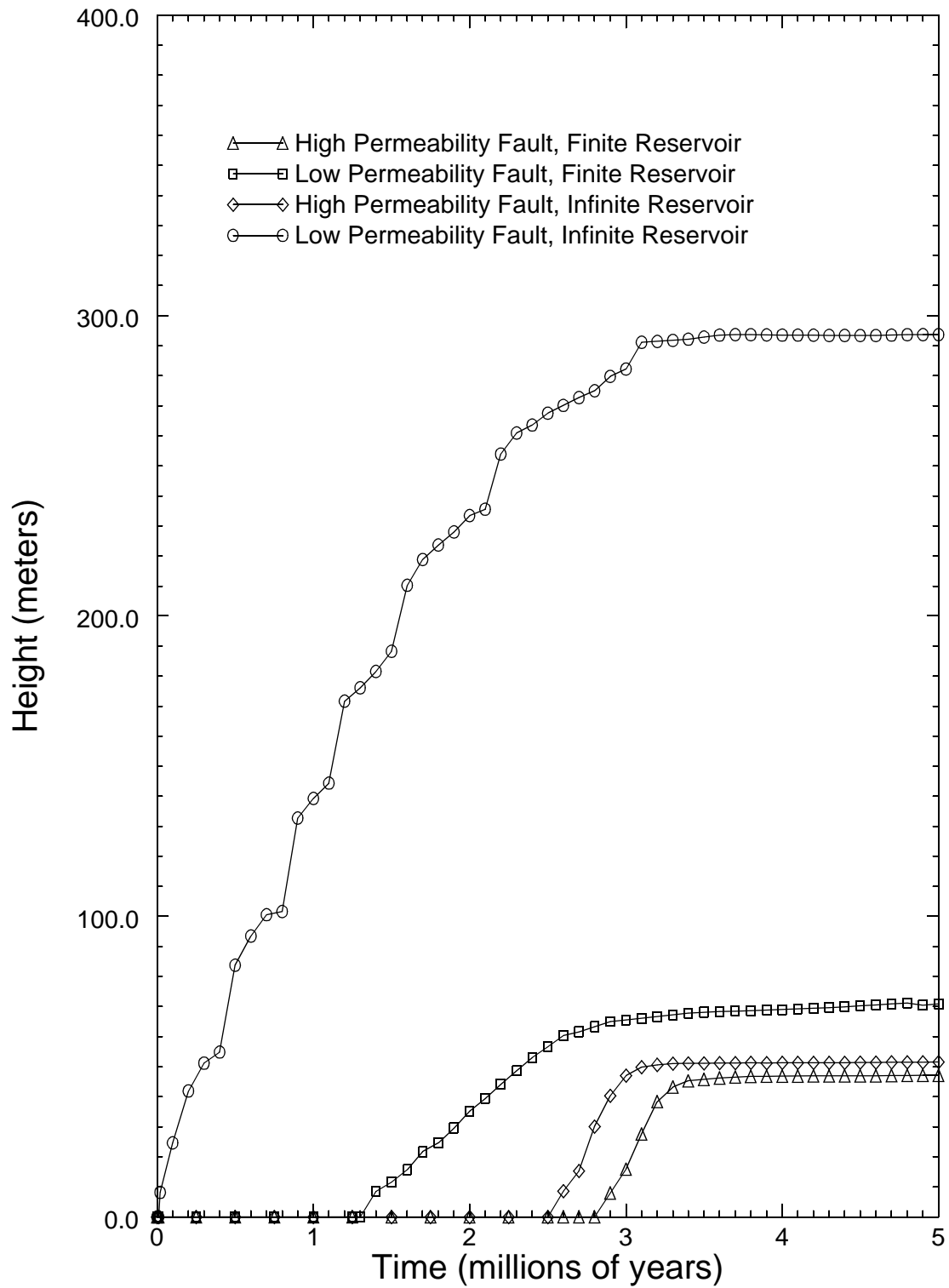
Figure 39. Hydrocarbon column height versus time for the complex fault and multiple reservoirs simulation (RUN_6).

Figure 39 illustrates that these reservoirs fill sequentially. The first reservoir (infinite reservoir attached to low permeability fault section) fills to approximately 50% of itÕs eventual steady-state column height before the second reservoir (finite reservoir attached to low permeability fault section) begins to fill (Figure 39). The second reservoir fills to approximately 80% of its eventual steady-state column height before the third reservoir (infinite reservoir attached to high permeability fault section) begins to fill. The third reservoir fills to approximately 58% of its eventual steady-state column height before the fourth reservoir (finite reservoir attached to high permeability fault section) begins to fill.

Figures 40 through 42 illustrate the transient response of oil saturation in this system as it is charging. Figure 42 has the steady state solution occurring at about 5.0 million years.
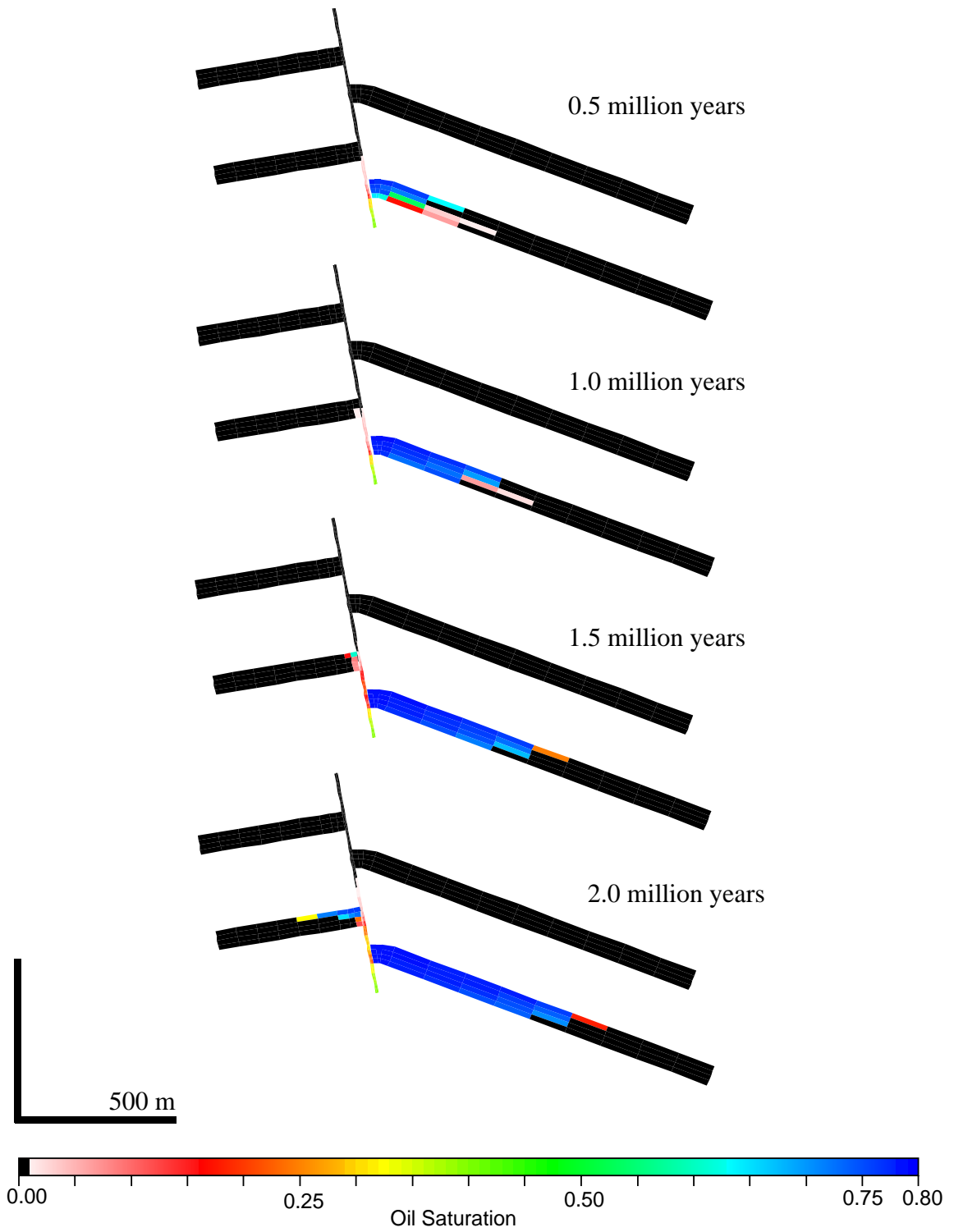
Figure 40. Saturation of oil versus location for RUN_6 at 0.50, 1.00, 1.50, and 2.00 million years.

2.5 million years

3.0 million years

3.5 million years

4.0 million years

500 m

0.00   0.25   0.50   0.75   0.80
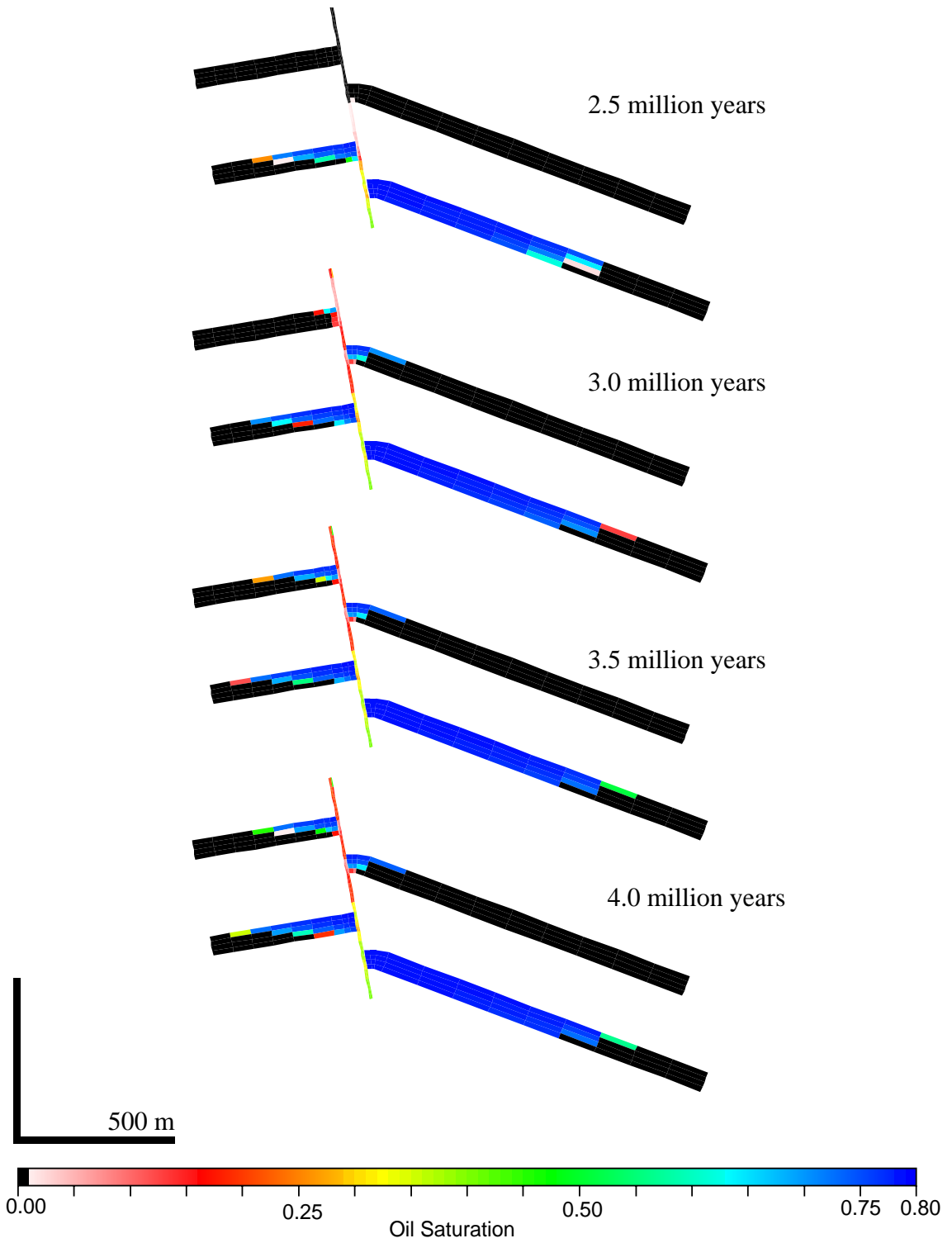
Oil Saturation

Figure 41. Saturation of oil versus location for RUN_6 at 2.50, 3.00, 3.50, and 4.00 million years.

4.5 million years

5.0 million years

500 m

0.00   0.25   0.50   0.75   0.80
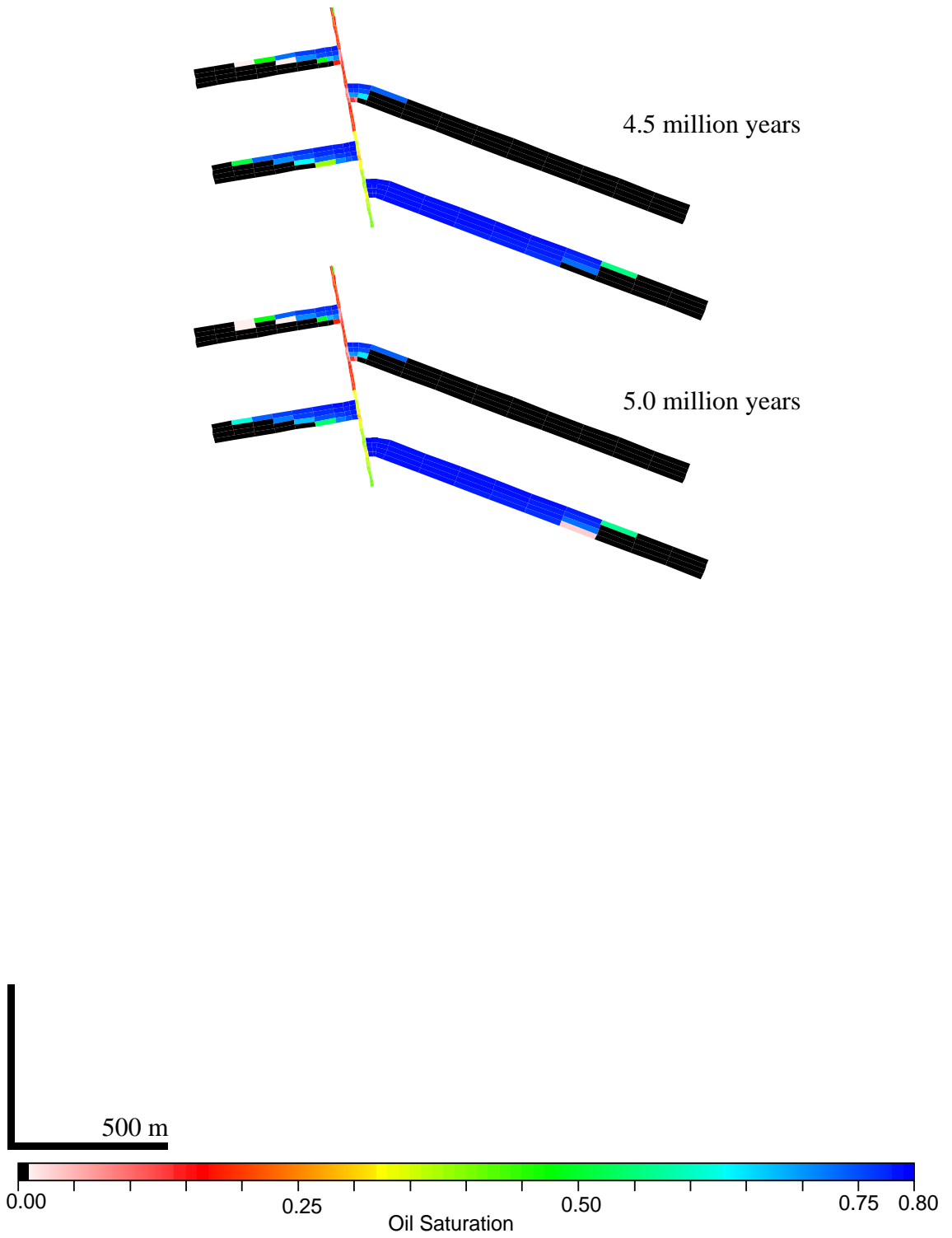
Oil Saturation

Figure 42. Saturation of oil versus location for RUN_6 at 4.50 and 5.00 million years.

Table 3: Key Input and Output for Simulations

	RUN_1	RUN_2	RUN_3	RUN_4	RUN_5	RUN_6
Fault k (mD)	0.10	0.10	0.10	0.01	0.01	0.10 Upper 0.01 Lower
Fault Porosity	0.05	0.05	0.05	0.05	0.05	0.05
Reservoir Type	Infinite	Infinite	Finite	Infinite	Finite	Finite and Infinite
Flux into Fault (m/s)	$1.13*10^{-12}$	$1.13*10^{-11}$	$1.13*10^{-11}$	$1.13*10^{-11}$	$1.13*10^{-11}$	$1.13*10^{-11}$
Numerical Column Height (m)	34	42	42	341	58	variable
Analytical Column Height (m)	35	44	44	347	347	variable
Numerical Time to Steady State	3.5 million years	1.0 million years	1.0 million years	10.0 million years	1.5 million years	5.0 million years
Analytical Time to Steady State	3.4 million years	0.5 million years	0.5 million years	5.8 million years	5.8 million years	

Discussion

From these six simulations it becomes evident that methodologies used in the past to predict hydrocarbon column height may, in some instances, prove to be less than adequate. Schowalter (1979), for example, states that the hydrocarbon column height is a function of the capillary pressure relationship for the fault zone whereby the Òbreak throughÓ saturation is static. This implies that a fault zone with a given capillary pressure relationship will trap hydrocarbon columns of the same height. The first simulation demonstrates SchowalterÕs static principle (Figure 48a). Our methodology, however, predicts that for a given fault zone the hydrocarbon column height is primarily dependent upon the flux of hydrocarbons into the fault, the saturation that results from this flux, and the capillary pressure in the fault zone at the specified saturation. This method allows for dynamic hydrocarbon column heights. That is, hydrocarbon column heights may vary for the same fault zone as a function of the flux into the fault. This principle is demonstrated with our second simulation (Figure 48b). The distinction lies in the process whereby hydrocarbons are put in place. SchowalterÕs model suggests that a seal overlying a reservoir charged from the bottom is only capable of trapping an oil column equivalent in height to the height predicted by a 10% oil saturation on the capillary pressure curve. Our model invokes the seal as the primary conduit for the emplacement of hydrocarbons into the reservoir. Furthermore, our model shows that the sealing capacity of a fault zone, or any sealing material for that matter, is a function of the oil saturation within the seal.

In addition to the dynamic response of hydrocarbon column height to flux, we consider the variation of hydrocarbon column height with respect to reservoir geometry. For small hydrocarbon column heights, relative to reservoir thickness, we observe that there is

little
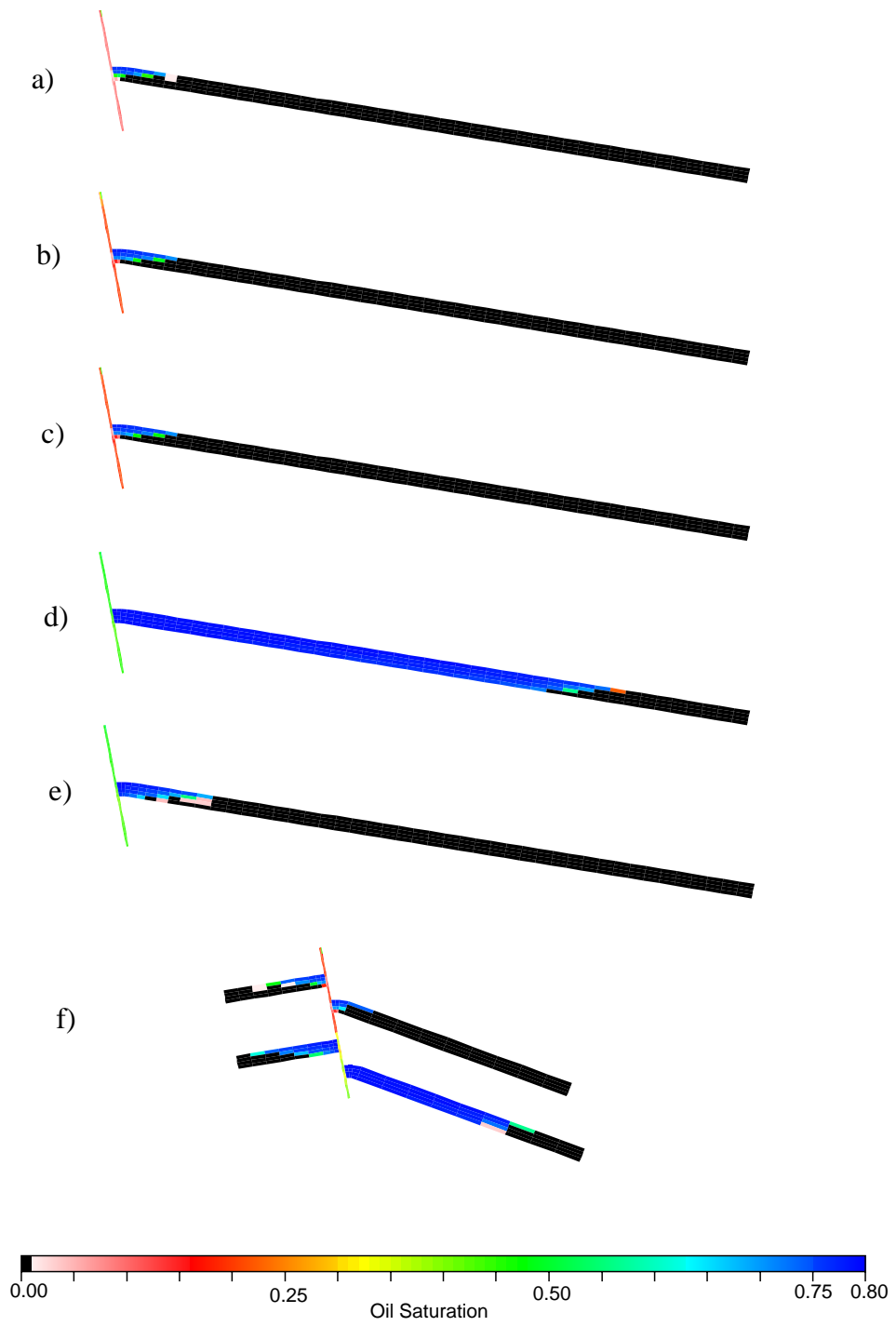
Figure 43. Summary of oil saturation versus location for the six simulations. a) RUN_1. b)

RUN_2. c) RUN_3. d) RUN_4. e) RUN_5. f) RUN_6.

if any difference in the hydrocarbon column height with variations in reservoir geometry. Comparing RUN_2 and RUN_3 we observe little or no variation in hydrocarbon column height (Figures 48b and 48c). For large hydrocarbon column heights relative to reservoir thickness, however, we observe large differences in oil column height as a function of reservoir geometry. For the same input parameters, a regional and infinite reservoir can support much larger hydrocarbon columns than a local and finite reservoir (Figures 48d and 48e). We observe that this is due primarily to the inability of water to exit the reservoir from the fault-reservoir interface. The relative permeability to water at this interface is effectively reduced to zero. This phenomena is referred to as Òperched waterÓ. As oil fills the reservoir, the water is displaced through the fault reservoir interface. Once the oil-water contact exceeds the thickness of the reservoir and the water saturations at the interface approach irreducible, the water is effectively locked into place. Since the water is essentially locked in the reservoir, oil is unable to infill. This implies that adequate structure is not the only criterion needed for a suitable hydrocarbon trap. In the case of a stratigraphic pinch out or sand lens, a suitable structure may exist that is capable of supporting large hydrocarbon columns. However, if connate water already in place is incapable of leaking out of the reservoir, the trap may never charge to itÕs full potential. This is largely due to the nearly incompressible nature of water. In small and finite reservoirs, the water in place may be slightly compressible, this compressibility, however, is not adequate to accommodate the amount of oil that could potentially charge the reservoir. In the case of large and infinite acting reservoirs, there is enough water to accommodate to oil that infills the updip portion of the trap.

Relatively complex systems are also considered in order to understand the controls on hydrocarbon columns associated with more realistic geological scenarios. RUN_6 reveals the sequential nature of filling reservoirs connected to the same fault and the spatial distribution of columns as a function of different boundary conditions and fault rock properties. We find that reservoirs attached to the same fault fill sequentially from the bottom up, that fault rock properties such as permeability directly affect the height of hydrocarbon columns and that the outer boundary conditions of these reservoirs can greatly affect the height of hydrocarbon columns where large columns, relative to sand thickness, are predicted.

References

Amyx, J.W., D.M.Bass, Jr., and R.L.Whiting, 1960, Petroleum Reservoir Engineering: New York, McGraw-Hill. 610 p.

Antonellini, M., and Aydin, A., 1994, Effect of Faulting on Fluid Flow in Porous Sandstones: Petrophysical Properties: AAPG Bulletin, v. 78, p. 35-377.

Bouvier, J.D., Kaars-Sijpesteijn, C.H., Kluensner, D.F., Onyejekwe, C.C., and Van der Pal, R.C., 1989, Three-Dimensional Interpretation and Fault Sealing Investigations, Nun River Field, Nigeria: AAPG Bulletin, v. 73, p. 1397-1414.

Ertekin, T.,Abou-Kassem, J. H., and King, G. R., 1993, Basic Applied Reservoir Simulation, Society of Petroleum Engineers Textbook Committee.

Forster, C.B., Goddard, J.V., and Evans, J.P., 1993, Permeability Structure of a Thrust Fault, in S. Hickman, R. Sibson, R. Bruhn, eds., USGS Proceedings of Workshop LXIII, The Mechanical Involvement of Fluids in Faulting: USGS Openfile Report 94-228, p. 216-223.

Hippler, S.J., 1993, Deformation Microstructures and Diagenesis in Sandstone Adjacent to an Extensional Fault: Implications for the Flow and Entrapment of Hydrocarbons: AAPG Bulletin, v. 77, p. 625-637.

Jordan, J.R., Campbell, F.L., 1984, Well Logging I-Rock Properties, Borehole Environment, Mud and Temperature Logging: New York, Society of Petroleum Engineers of AIME, 167 p.

Katz, A. J. and Thompson, A. H., 1986, Quantitative Prediction of Permeability in Porous Rock: Physical Review B, v. 34, p. 8179-8181.

Knipe, R.J., 1992, Faulting Processes and Fault Seal, in R.M. Larsen, H. Brekke, B.T. Larsen and E. Talleraas, ed., Structural and Tectonic Modelling and its Application to Petroleum Geology, NPF Special Publication 1, p. 325-342.

Pittman, E.D., 1981, Effect of Fault-Related Granulation on Porosity and Permeability of Quartz Sandstones, Simpson Group (Ordovician), Oklahoma: AAPG Bulletin, v. 65, p. 2381-2387.

Scholz, C.H., and Anders, M.H., 1993, The Permeability of Faults, in S. Hickman, R. Sib-

son, R. Bruhn, eds., USGS Proceedings of Workshop LXIII, The Mechanical Involvement of Fluids in Faulting: USGS Openfile Report 94-228, p. 216-223.

Schowalter, T. T., 1979, Mechanics of Secondary Hydrocarbon Migration and Entrapment: AAPG Bulletin, v. 63, p. 723-760.

Smith, Derrell A., 1966, Theoretical Considerations of Sealing and Non-sealing Faults: AAPG Bulletin, v. 50, p. 363-374.